Contents lists available at ScienceDirect

Tectonophysics

journal homepage: www.elsevier.com/locate/tecto

Evolution of fluid pathways during eclogitization and their impact on formation and deformation of eclogite: A microstructural and petrological investigation at the type locality (Koralpe, Eastern Alps, Austria)

A. Rogowitz [a,*], B. Huet [b]

[a] *Department of Geology, University of Vienna, Vienna, Austria*
[b] *Department of Hard Rock Geology, Geological Survey of Austria, Vienna, Austria*

ABSTRACT

Eclogites representing three strain stages from the type locality (Saualpe-Koralpe Complex, Eastern Alps, Austria) have been analyzed with regard to their microstructural, petrological and mechanical evolution during the gabbro-eclogite transformation and subsequent deformation. Thermodynamic forward models suggest the presence of a H_2O dominated fluid phase during eclogitization and following deformation. While all three eclogite types show the same mineral paragenesis composed of garnet, omphacitic clinopyroxene, quartz and a fine grained polyphase aggregate of kyanite, clinozoisite, quartz and retrograde plagioclase, we do observe a microstructural and mechanical evolution with strain.

Eclogitization is controlled by dissolution of metastable gabbro and precipitation of the stable finer grained eclogitic mineral paragenesis. This induces a micro-porosity which allows fluids to migrate in an unchannelized way. Distributed eclogitization results in strain weakening, where both transformational and volumetric strain are accommodated by dissolution-precipitation creep. Subsequent deformation of eclogite results in the development of pronounced eclogitic foliation accompanied by grain coarsening and reduction of porosity. The latter results in a reduced efficiency of dissolution-reprecipitation possibly causing apparent strain hardening. Based on our observations we suggest a model for the rheological evolution during the transformation of a dry mafic rock into an eclogite where the combination of volumetric and transformational strain at the onset of eclogitization assisted by fluid induces rapid weakening followed by apparent hardening once eclogitization is completed and steady state deformation of the eclogite mineral paragenesis sets in.

1. Introduction

Eclogite forms during high to ultra-high pressure metamorphism of mafic rocks like basalt, gabbro and granulite (Austrheim, 2013 and references therein) and as such provides an essential record of the processes active at a wide range of scales in subduction and collision zones. Additionally, the presence of potentially large volumes of eclogite in the buried oceanic crust and lower continental crust makes the small scale processes controlling their formation and deformation relevant for the mechanics and dynamics of convergent plate boundaries at different time scales (Jolivet et al., 2005; Labrousse et al., 2010; Agard et al., 2018, 2020). Even though the classical eclogite assemblage consists of the non-hydrous minerals garnet and omphacite, it is widely accepted that the transformation of a mafic protolith into an eclogite requires

fluid infiltration (Austrheim, 1987; Pennacchioni, 1996; Austrheim et al., 1997; John and Schenk, 2003; Jolivet et al., 2005; Engvik et al., 2007; Cao et al., 2020). While the role of fluids acting as a catalyst for metamorphic reactions seems to be a common observation, the actual processes by which fluid enhances eclogitization are still under debate. For example, it has been suggested that fluid can enhance solid-state diffusion (Schorn, 2018) and activation of dissolution and precipitation creep (Putnis and Austrheim, 2010; Giuntoli et al., 2018). Further, it must be distinguished whether the fluid acts solely as a kinetic catalyst allowing for more efficient solid-state mechanisms to be active (Putnis and Austrheim, 2010) or if it plays an additional thermodynamic role by providing elements and/or changing chemical potential gradients (John and Schenk, 2003; Putnis and Austrheim, 2010).

While the necessity of fluids during eclogitization of mafic dry

---

protolith seems to be inevitable, the pathways by which fluids can infiltrate are variable. Fractures forming during deep-seated earthquakes are one of the most commonly proposed fluid pathways (Austrheim et al., 2017; Putnis et al., 2017; Petley-Ragan et al., 2018; Jamtveit et al., 2019). Such fractures do not only allow fluid infiltration in the dry mafic protolith but can also act as precursors for localization of ductile strain (Segall and Simpson, 1986; Mancktelow and Pennacchioni, 2005; Raimbourg et al., 2005; Goncalves et al., 2016; Menegon et al., 2017). Highly localized shear zones can then enhance fluid pathways by activation of creep cavitation related to grain boundary sliding and phase mixing (Fusseis et al., 2009; Gilgannon et al., 2017). Another possible way for fluid to infiltrate the protolith is the density increase during eclogitization. The resulting volume decrease is often associated with fracturing and development of porosity resulting in a self-driven process once being kicked-off (Austrheim, 1987; Engvik et al., 2007).

Besides its crucial role in the kinetics of metamorphic reactions, fluid also plays an important role during deformation and strain localization in eclogite. For example, the rather unexpected weakness of eclogite showing localized shear zones and strongly foliated eclogite mylonites is often associated with reaction induced softening promoted by the presence of fluids and development of weaker hydrated phases like (clino-)zoisite and mica (Engvik et al., 2007; Stünitz and Tullis, 2001). Nevertheless, foliated eclogite consisting almost exclusively of garnet and omphacite can also show a strong foliation, which reflects hydrolytic weakening promoting mobility of dislocations in dislocation creep (Griggs, 1967) or mass in diffusion creep (Brodie and Rutter, 1987; Stünitz et al., 2020) rather than metamorphic reaction induced softening.

In this contribution, we present a detailed petrographical, microstructural and chemical study on a set of eclogites representing three strain stages, collected at the outcrop of Hohl (Miller and Thöni, 1997; Bruand et al., 2010) that is part of the eclogite type locality (Fig. 1, Saualpe-Koralpe Complex, Eastern Alps, Austria). The investigations reveal that the formation of eclogite at close to static conditions resulted in the development of a porosity at high pressures, which allowed for dispersed fluid infiltration. Continuous supply of a H_2O dominated fluid phase assisted eclogitization by the activation of dissolution precipitation processes. However, subsequent deformation of eclogite appears to be accompanied by a reduction in porosity and apparent strain hardening. The observed negative feedback between deformation and fluid pathways contradicts previous studies in which deformation is considered to introduce porosity (Engvik et al., 2007; Fusseis et al., 2009; Gilgannon et al., 2017). Eventually, the presented data allows us to link fluid assisted microstructural processes to possible large scale softening and hardening evolution in eclogitized dry mafic rocks.

2. Geological setting

The Saualpe-Koralpe Complex (SKC) is a polymetamorphic crystalline basement belonging to the Austroalpine Unit of the Eastern Alps (Miller et al., 2005). It represents the largest unit of the Alps that experienced high-pressure metamorphism during the Cretaceous (Bruand et al., 2010). The Saualpe and Koralpe ranges are known as the eclogite type locality (Haüy, 1822) and comprises about 200 metagabbro and eclogite lenses, varying in size from one to several hundreds of meters, embedded in micaschist, gneiss, marble and amphibolite (Miller, 1990; Tenczer and Stüwe, 2003; Thöni et al., 2008; Bruand et al., 2010).

Before the Cretaceous orogeny, the SKC experienced Permian high-temperature metamorphism related to lithospheric extension, formation of the Adriatic continental margin and opening of the Tethys Ocean (Habler and Thöni, 2001; Schuster and Stüwe, 2008). Peak conditions are estimated to lie in the range 0.38–0.65 GPa and 600–650 °C and were reached between 270 and 250 Ma (Habler and Thöni, 2001; Schulz, 2017). Permian rifting was accompanied by the emplacement of N-MORB gabbro and possibly basalt, which served as eclogite protoliths especially in the SKC (Thöni and Jagoutz, 1992; Miller et al., 2007).

Late Jurassic to Cretaceous convergence led to intracontinental subduction at the Adriatic continental margin together with accretion and widespread metamorphism of the continental material forming the Austroalpine Unit (Miller et al., 2007; Stüwe and Schuster, 2010). Within the SKC, peak metamorphism occurred at 95–94 Ma (Thöni, 2006; Thöni et al., 2008) and at conditions falling in the range 1.5–2.2 GPa and 620–740 °C inferred from thermodynamic modeling (Bruand et al., 2010; Schorn and Diener, 2017; Schorn, 2018) and conventional thermobarometry (Gregurek et al., 1997; Miller et al., 2005). It was followed by rapid, near-isothermal decompression from 90 to 88 Ma onwards (Miller et al., 2005; Thöni et al., 2008). The processes resulting in the exhumation of the SKC are still under debate and several models have been proposed, one of them being related to slab extraction (Froitzheim et al., 2003). Others link eclogite exhumation to the formation of the Plattengneiss shear zone (Kurz et al., 2002; Wiesinger et al., 2006), which is a 250–600 m thick presently flat lying mylonitic shear zone (Putz et al., 2006). A recent study suggests a combination of slab extraction and erosional exhumation (Schorn and Stüwe, 2016).

3. Methods

3.1. Microstructural analysis

Samples have been cut in the apparent XZ plane of finite strain in order to prepare mechanically polished thin sections with a thickness of

Fig. 1. Photographs of the Koralpe eclogites. a. Polished rock at the *Geopark Glashütten* showing the transition from gabbro to eclogite. The white dashed line traces the reaction front. Gabbro and eclogite are crosscut by late fractures (black arrows) that are locally reactivated as shear zones (white arrows). Black rectangle shows locality of inserted close up. b. Coronitic eclogite showing garnet coronae (red) around magmatic clinopyroxene (dark green) in a matrix of omphacitic clinopyroxene (light green) and clinozoisite-kyanite-quartz fine grained aggregate (white). Width of the picture: 4 cm. Coordinates: 46°43′32″N 15°08′44″E. c. Highly foliated eclogite showing elongated garnet aggregates (red) in a matrix of omphacitic clinopyroxene (green) with small amount of clinozoisite-kyanite-quartz aggregate (white). Width of the picture: 7 cm. Coordinates: 46°43′49"N 15°8′46″E. (For interpretation of the references to colour in this figure legend, the reader is referred to the web version of this article.)

about 30 μm. Phase relations, modal composition and microstructure have first been analyzed using a Leica DM4500 P polarization microscope. Thin sections selected for scanning electron microscopy (SEM) and electron microprobe (EMP; Table 1,) analyses have been carbon coated in order to establish conductivity. Thin sections selected for electron backscatter diffraction (EBSD) have been chemo-mechanically polished for a minimum of 3 h with an alkaline colloidal silica suspension (Syton©).

Mineral chemistry has been measured with a CAMECA SX Five SE electron microprobe at the Department of Lithospheric Research (University of Vienna, Austria). The microprobe has been operated at an acceleration voltage of 15 kV, a beam current of 20 nA. Plagioclase has been analyzed with a beam defocus of 5 μm. Structural formula have been calculated using the MINSORT software (Petrakakis and Dietrich, 1985).

EBSD mapping has been performed in order to quantify the amount of intracrystalline distortion and detect possible crystallographic preferred orientation (CPO). Analyses have been performed on a FEI Quanta 3D FEG scanning electron microscope equipped with SE-, BSE-, EDX- and EBSD-detectors at the Department for Lithospheric Research (University Vienna, Austria). The SEM was operated at an accelerating voltage of 15 kV, a beam current of 4 nA in analytical mode, a working distance of 14 mm and a sample tilt of 70°. The step size between 2.8 and 3.5 μm was adapted in order to detect a representative number of grains. The OIM Data Collection and Analysis software was used for indexing and processing the EBSD data. Data have been cleaned based on the confidence index (CI > 0.1). Orientation distribution functions (ODFs) were calculated following Bunge (1982) and plotted as equal angle upper hemisphere projections. The data is also plotted as grain-averaged misorientation maps and misorientation-deviation angle maps representing the misorientation of each pixel with respect to the grain-averaged misorientation. Data obtained from EBSD analysis on grain shape and orientation have been the base for aspect ratio analysis (AR: short axis divided by grain long axis).

Representative eclogite samples have been cut into ~0.5 cm thick slices and broken approximately in the apparent XY, YZ and XZ planes of finite strain in order analyze mineral surfaces with the FEI Quanta 3D FEG scanning electron microscope of the Department for Lithospheric Research. All sides of broken samples have been carbon coated to establish conductivity. The SEM has been operated at an acceleration voltage of 15 kV and a working distance of 8 to 14 mm. Qualitative chemistry analysis with energy dispersive X-ray spectroscopy has been performed using the EDAX-Team software for mineral identification.

3.2. Thermodynamic forward modeling

Thermodynamic forward modeling was carried out with the Theriak-Domino software package (de Capitani and Brown, 1987; de Capitani and Petrakakis, 2010) for determining the pressure-temperature conditions and water activity during eclogitization as well as calculating rock density. We used the thermodynamic database compiled by Doug Tinkham (http://dtinkham.net/td-6axNCKFMASHTOm45.txt.zip, version 4 of May 27, 2018) which includes the version ds6.2 of the thermodynamic dataset of Holland and Powell (2011). Calculations were done in the NCFMASHTO system with the following activity models: clinopyroxene (model CPXG16 for calculations at high pressure

Table 1
Representative electron microprobe analyses of minerals in Al-Mg-rich eclogite from the outcrop of Hohl.

	Garnet			Omphacitic clinopyroxene			Clinozoisite			Plagioclase		
	Low strain	Intermediate strain	High strain	Low strain	Intermediate strain	High strain	Low strain	Intermediate strain	High strain	Low strain	Intermediate strain	High strain
SiO2	39,656	40,110	40,033	54,265	54,628	54,641	39,335	39,332	38,834	62,402	62,817	61,562
TiO2	0,038	0,040	0,032	0,189	0,151	0,168	–	–	–	0,021	0,004	0,007
Al2O3	22,789	22,498	22,690	8,114	8,436	8,593	32,562	32,657	32,601	23,696	23,586	21,950
Cr2O3	0,043	0,000	0,230	0,113	0,000	0,288	0,098	0,000	0,174	–	–	
FeO	17,844	17,777	17,695	2,937	2,542	2,324	1,276	1,103	0,990	0,066	0,111	0,371
MgO	10,795	11,057	10,957	12,191	11,579	11,708	0,065	0,084	0,071	0,003	0,000	1481
MnO	0,479	0,495	0,475	0,035	0,033	0,018	0,008	0,000	0,004	0,000	0,000	0,010
CaO	8,677	8,250	8,336	19,158	18,676	18,111	24,572	24,955	24,643	4,961	4,844	6,027
Na2O	–	–	–	3,208	4,047	4,147	–	–	–	8,987	8,995	8,551
K2O	–	–	–	0,000	0,000	–	–	–	–	0,000	0,000	0,009
Total	100,321	100,227	100,448	100,210	100,092	99,998	97,916	98,131	97,317	100,136	100,357	99,968
Oxygen	12	12	12	6	6	6	25	25	25	8	8	8
Si	2,963	2,992	2,983	1,943	1,952	1,952	5,978	5,963	5,933	2,761	2,771	2,746
Al_IV	0,037	0,008	0,017	0,057	0,048	0,048	5,832	5,835	5,870	1,235	1,226	1,154
Al_VI	1,970	1,971	1,976	0,285	0,307	0,314						
Ti	0,002	0,002	0,002	0,005	0,004	0,005		0,000	–	0,001	0,000	0,000
Cr	0,003	0,000	0,014	0,003	0,000	0,008	0,012	0,000	0,021	–	–	
Fe3+	0,025	0,027	0,008	0,000	0,013	0,004	0,162	0,128	0,126	0,002	0,004	0,014
Fe2+	1,090	1,082	1,095	0,088	0,063	0,065	0,000	0,000		0,000	0,000	0,000
Mg	1,202	1,230	1,217	0,651	0,617	0,623	0,015	0,019	0,016	0,000	0,000	0,000
Mn	0,030	0,031	0,030	0,001	0,001	0,001	0,001	0,000	0,001	0,000	0,000	0,000
Ca	0,695	0,659	0,666	0,735	0,715	0,693	4,001	4,000	4,034	0,235	0,229	0,288
Na	–	–	–	0,223	0,280	0,287	–	–	–	0,771	0,769	0,739
K	–	–	–	0,000	0,000	–	–	–	–		0,000	0,001
Total	8,017	8,002	8,008	3,991	4,000	4,000	16,001	15,945	16,001	5,005	4,999	4,942
Xalm	0,366	0,365	0,367									
Xprp	0,405	0,416	0,409									
Xgrs	0,219	0,208	0,214									
Xsps	0,010	0,010	0,010									
Q (wo, en, fs)				0,715	0,682	0,681						
ae				0,000	0,013	0,004						
jd				0,223	0,269	0,279						
cats				0,062	0,036	0,035						
Xab										0,766	0,771	0,656
Xan										0,234	0,229	0,343
Xo										0,000		0,000

and AUGG16 for calculations at low pressure, Green et al., 2016), garnet (model GRTW14, White et al., 2014), clinoamphibole (model CAMPG16, Green et al., 2016), clinozoisite (model EP11, Holland and Powell, 2011) and plagioclase (model PlHP, Holland and Powell, 2003).

The chemical composition used as input was determined as follows. We selected six thin sections representative of Al-Mg-rich eclogite from the Hohl locality. These thin sections cover the whole range of deformation intensity. They were scanned with a micro-XRF M4 TORNADO instrument (Brucker) at University of New Brunswick (Canada). The difference between analyses are small and do not correlate with deformation. An average composition was then calculated by taking the arithmetic mean of the six analyses, yielding SiO_2: 48.51, TiO_2:0.38, Al_2O_3: 16.88, Cr_2O_3: 0.21, Fe_2O_3: 6.03, MnO: 0.10, MgO: 9.17, CaO: 16.43, Na_2O: 2.15, K_2O: 0.00 (values in wt%). This composition is similar to the published analyses of gabbro and kyanite-bearing eclogite from the SKC (Miller et al., 1988; Miller and Thöni, 1997). These rocks are characterized by high Al, Mg and Ca content and are interpreted to originate in cumulates derived from a tholeiitic magma (Miller et al., 1988; Miller and Thöni, 1997). For thermodynamic forward modeling, minor elements (Cr, Mn, K) were discarded. Exclusion of Mn from the considered system is justified by the very low spessartine content and the absence of distinct Mn zonation in garnet (see Section 4.1). The proportion of ferric iron was fixed to $Fe^{3+}/Fe_{tot} = 0.15$ (Palin et al., 2016). This allowed a good match between the amount of Fe^{3+} measured in silicates and the calculated one ($XFe^{3+} = Fe^{3+}/(Al + Fe^{3+})$ < 0.01 in garnet, $XFe^{3+} = Fe^{3+}/(Al + Fe^{3+}) \sim 0.10$ in clinopyroxene and $XFe^{3+} = Fe^{3+}/(Al + Fe^{3+}-2) = 0.07–0.10$ in clinozoisite). H_2O was treated as a component with variable activity. Considering H_2O activity instead of H_2O content allows to model simply a fluid that is a mixture of H_2O and other components (CO_2, NaCl, …) without having to account for those explicitly in the calculation.

The equilibrium assemblage and phase chemistry was calculated for discrete values of pressure (P) between 1 and 3 GPa, temperature (T) between 600 and 800 °C and H_2O activity (a(H_2O)) between 0.1 and 1. The pressure, temperature and activity resolutions were set to 0.01 GPa, 2 °C and 0.005 respectively. The considered P-T range is large enough to encompass the variety of conditions determined for the pressure peak in the SKC (Gregurek et al., 1997; Miller et al., 2005; Bruand et al., 2010; Schorn and Diener, 2017; Schorn, 2018). The composition of garnet and clinopyroxene determined by Theriak-Domino at each P-T-a(H_2O) condition was systematically compared to the inferred equilibrium one measured with the electron microprobe. Five chemical parameters characterizing the compositions were considered: $XFe = Fe/(Fe + Mg + Ca)$, $XMg = Mg/(Fe + Mg + Ca)$, $XCa = Ca/(Fe + Mg + Ca)$ in garnet and $XNa = Na/(Na + Ca)$ and XMg $Mg/(Fe + Mg)$ in clinopyroxene. For each compositional parameter, we calculated the absolute difference between the measured and the calculated value and tested if it remains below a given tolerance (0.05: poor fit, 0.005: very good fit). These five quantitative tests allowed us to estimate as precisely as possible the P-T-a (H_2O) conditions recorded in the investigated samples.

4. Petrographical, microstructural and chemical analysis

The eclogites of the SKC have been extensively studied in terms of their origin, petrology and metamorphic conditions (Tenczer and Stüwe, 2003; Miller et al., 2005; Miller et al., 2007; Bruand et al., 2010; Proyer and Postl, 2010; Schorn and Diener, 2017; Schorn, 2018). Two types of N-MORB protoliths are distinguished based on the Mg content (Miller et al., 2007). Low-Mg eclogite is dominated by omphacite, garnet, quartz and amphibole whereas Al-Mg-rich eclogite additionally contains clinozoisite and kyanite (Miller et al., 2007; Bruand et al., 2010). In the present study, we focus on microstructures and petrology of the Al-Mg-rich eclogite from the locality of Hohl in the Koralpe range (coordinates: 46°43′49″N 15°8′45.92″E, Miller and Thöni, 1997; Bruand et al., 2010). Samples were collected within a few tens of meters along a strain gradient showing an increasing development of eclogitic foliation and

lineation from bottom to top where the top represents the rim and the bottom is the center of a large eclogite body. Notice that the strain evolution could not be continuously documented because of the bad exposure in the forest.

Mineral abbreviations in the text and figures are taken from Whitney and Evans (2010). All three eclogite types are composed of the same mineral paragenesis composed of garnet (grt), omphacitic clinopyroxene (cpx), quartz (qtz) and a fine grained polyphase aggregate of kyanite (ky), clinozoisite (czo), quartz (qtz) as well as retrograde plagioclase (pl), which will be referred to as fgpa. Minor amphibole (amp) and rutile (rt) also occur. The following section focuses on a microstructural and petrological analysis of the eclogite samples representing three different strain stages. While the mineral assemblage is similar in all investigated samples, we observe a variation in the petrography and microfabric of the three eclogite types. Petrographical observations, phase chemistry, the characteristics of grain surfaces and crystallographic orientations of each eclogite type are separately described in the following.

4.1. Petrography and phase chemistry

4.1.1. Low strain eclogite

Low strain eclogite is characterized by a coronitic fabric, where polycrystalline garnet coronae surround clinopyroxene in a matrix of fgpa and clinopyroxene (Figs. 2a, SF.1, SF.2). At the outer side of the corona, garnet crystals tend to be coarser grained ($\sim$500 µm) and show crystal faces growing towards the matrix, whereas rather fine garnet grains ($\sim$20 µm) and intergrowths with clinopyroxene develop towards the corona center. Even though coronae are made up of polycrystalline garnet aggregates, a continuous inclusion trail mainly composed of fine kyanite needles, minor clinozoisite, clinopyroxene and quartz can be
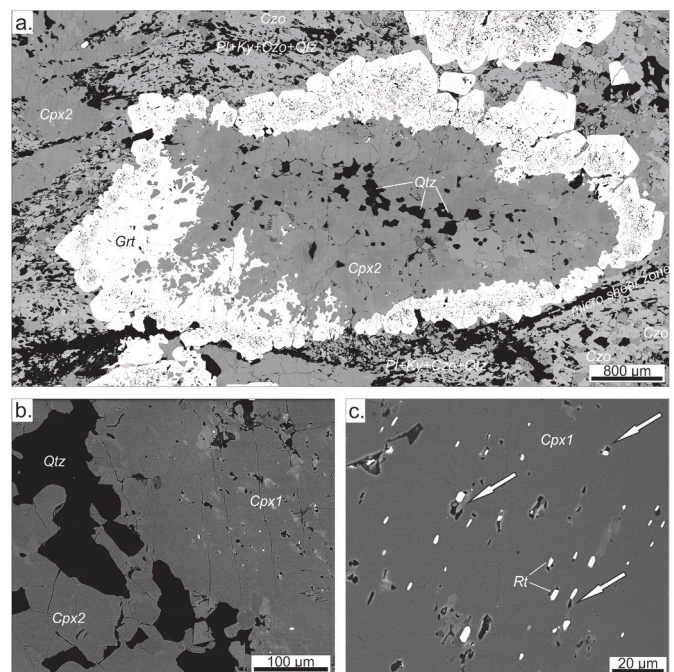

Fig. 2. Electron backscatter images of low strain eclogite. a. Garnet corona around omphacitic clinopyroxene, amphibole and quartz surrounded by a fine grained mixture of kyanite, clinozoisite and plagioclase with local enclaves of omphacitic clinopyroxene. Garnet shows inclusion-free coarse-grained crystal faces towards the matrix whereas clinopyroxene-garnet intergrowths can be observed towards the corona center. b. Reaction front between older clinopyroxene (cpx1) and omphacitic clinopyroxene (cpx2), quartz and amphibole. Note the micro-pores of cpx1 clinopyroxene often located close to rutile inclusions. c. Close up of cpx1 with rutile inclusions and micro-porosity (white arrows).

traced through entire coronae (Fig. 2a). Towards the coronae center solely minor resorbed clinopyroxene can be observed (SF.1c) while the outermost rim is always inclusion free (SF.1d).

Within the corona center, two different clinopyroxene fabrics are observed. Cpx1 corresponds to coarse grained (>800 μm) clinopyroxene with lobed grain boundaries and minor rutile inclusions aligned in parallel lines. In contrast, cpx2 clinopyroxene has a grain size ranging between 10 and 150 μm and shows an almost foam like structure (average AR: 0.5, mode AR: 0.7) with straight grain boundaries and grain triple junctions with nearly 120° angles (Fig. 3a). It occurs in a
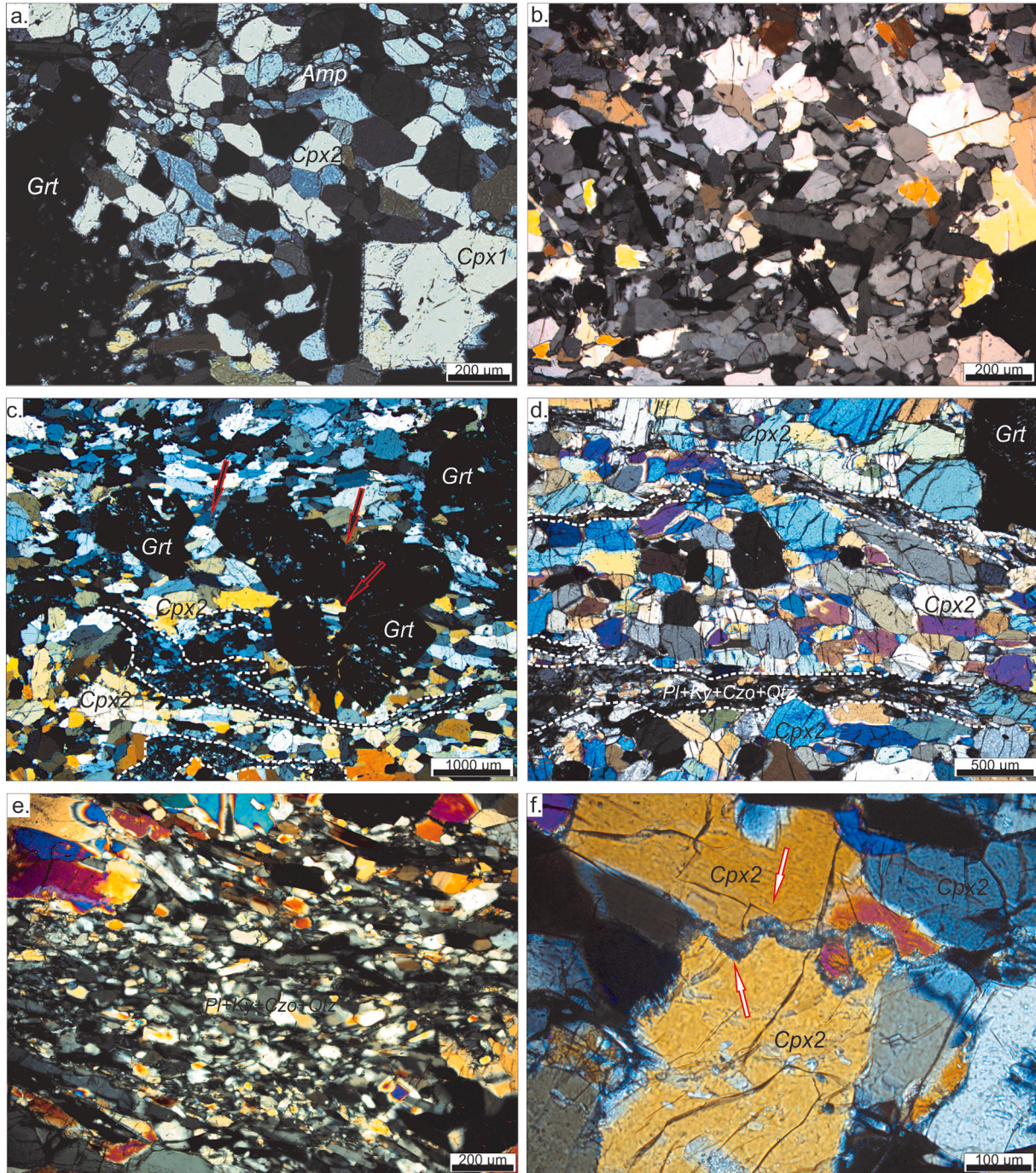
Fig. 3. Representative optical micrographs (crossed polarized light) of low strain (a, b), intermediate strain (c) and high strain (d- f) eclogite. a. Foam microstructure in omphacitic clinopyroxene and minor amphibole in a corona center. Left side of the image shows a garnet-clinopyroxene intergrowth. b. Fine grained mixture of kyanite, clinozoisite, clinopyroxene, quartz and plagioclase. Note the random shape orientation of the minerals. c. Onset of garnet-aggregate disaggregation in an omphacitic clinopyroxene dominated matrix. At areas of disaggregation, newly reprecipitated omphacitic clinopyroxene and quartz show a shape preferred orientation consistent with the extensional direction (black arrows). The fine-grained polyphase aggregate of kyanite, clinozoisite and quartz is arranged in patches and layers (delineated by white dashed lines) d. Omphacitic clinopyroxene showing a strong shape preferred orientation parallel to the foliation. The fine-grained polyphase aggregate of kyanite, clinozoisite and quartz (delineated by white dashed lines) is intercalated in layers subparallel to the foliation. Foliation perpendicular cracks are visible in omphacitic clinopyroxene. e. Fine grained mixture of clinozoisite, quartz, clinopyroxene, minor kyanite and plagioclase. Note the well-pronounced shape preferred orientation of the grains. f. Indenting omphacitic clinopyroxene grains traced by symplectite (white arrows).

mixture together with minor quartz and amphibole (Figs. 2a, 3a). Locally, transition from one fabric to the other can be observed in the form of cpx2-qtz intergrowths replacing the earlier cpx1 (Fig. 2b, SF.2). The fabric of cpx2 often shows cavities and open grain boundaries along intergrowths whereas cpx1 has a high density of micro-pores aligned with rutile (Fig. 2b, c).

Matrix grains of the fgpa are relative fine grained and have mostly a random orientation (Fig. 3b). Locally clinozoisite dominated areas can be observed within the fgpa (Fig. 2a). In those rather monomineralic areas clinozoisite can reach a diameter of up to 200 μm. Despite the occurrence of these monomineralic areas, clinozoisite only occurs in the fgpa (pl + ky + czo + qtz) outside of coronae. Elongated polycrystalline aggregates of cpx2 locally occur in the matrix (Fig. 2a). These aggregates have a foam-like microstructure with straight grain boundaries similar to cpx2 within coronae. In corona-rich areas, strain can be localized along micro shear zones (SF.3). Such shear zones only localize within the fgpa and between coronae. They cannot be linked to a preferred kinematic framework. Minor symplectite with plagioclase and late clinopyroxene (cpx3) surround cpx2 crystals from coronae and matrix (SF.4a, ST.1).

Garnet has an average composition with Xprp = 0.4, Xalm = 0.37, Xgrs = 0.22 and Xsps = 0.01 (Table 1) and shows minor chemical zoning (Fig. 5a, 6a, b). At the interface between large garnet crystals and fine grained garnet crystals growing towards coronae center, the grossular content is perturbed. It shows an abrupt drop to the outer corona rim and a smoother decrease towards the center (Fig. 6a). Both clinopyroxene types (cpx1 and cpx2) are sodic. The composition of cpx1 is sodium poorer and rather variable with XNa = 0.10–0.25 and XMg = 0.89–0.95. In comparison, the composition of cpx2 is omphacitic and shows a more homogeneous composition with XNa = 0.26–0.29, XMg = 0.88–0.90 (Table 1, Fig. 5a). Clinozoisite has a homogeneous composition with 10–15% of epidote end member. Plagioclase in symplectite together with diopsidic clinopyroxene (XNa < 0.15, XMg ~ 0.9) and retrograde plagioclase in the fgpa are sodium-rich and contain 0.71 to 0.78 albite fraction (Table 1).

4.1.2. Intermediate strain eclogite

Intermediate strain eclogite is characterized by elongated and stretched garnet aggregates within a foliated clinopyroxene matrix. The grain size distribution of garnet does not show the wide range observed in the low strain eclogite and only large garnets are observed (~500–1000 μm). The garnet of those aggregates has a high density of inclusions (czo, ky and qtz, Fig. 3c, 4a). Garnet aggregates show incipient dismembering, preferentially perpendicular to the foliation along grain boundaries (Fig. 3c). Quartz, kyanite, clinozoisite and clinopyroxene often occur along newly developed interfaces (Figs. 3c, 4a, b). In areas where greater space between dismembered garnet aggregates developed, clinopyroxene crystals do have a preferred orientation with grain long axis parallel to the extensional direction (Fig. 3c). Amphibole is very rarely observed at these locations.

Clinopyroxene grains form most of the matrix and are of type cpx2 (~50–300 μm). They are more elongated than in the low strain eclogite (average AR: 0.43, mode AR: 0.55) and develop a shape preferred orientation (SPO) defining the foliation together with the stretched aggregates (Fig. 3c). Clinopyroxene of type cpx1 with rather coarse grains, lobed grain boundaries and minor undulatory extinction could only be found at locations entirely surrounded by garnet.

The fine-grained polyphase aggregate occurs either as patches close to elongated garnet aggregates or as layers within the clinopyroxene matrix. In the matrix fgpa, clinozoisite and kyanite show a weak SPO parallel to the one of clinopyroxene. In contrast to samples from low strain eclogite we here observe clinozoisite locally outside the fgpa assemblage resorbed by garnet aggregates (Fig. 4a). Retrograde plagioclase overgrows most minerals of the fgpa. Diopside-plagioclase symplectite overgrows cpx2 clinopyroxene from all microstructural positions (Fig. 4a; SF.4b, ST.1).
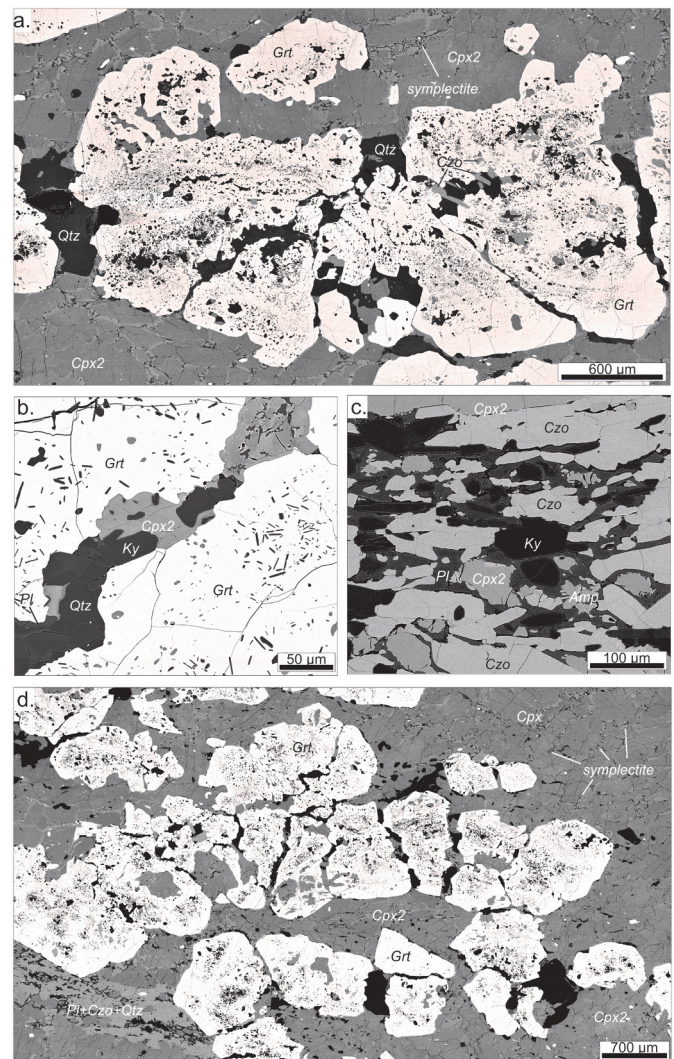

Fig. 4. Electron backscatter images of strained eclogite. a. Elongated inclusion-rich garnet aggregate in a matrix of recrystallized omphacitic clinopyroxene. Locally, plagioclase-diopside symplectite occur along omphacitic clinopyroxene grain boundaries. b. Garnet interphase showing eclogitic mineral paragenesis composed of omphacitic clinopyroxene, kyanite and quartz. Locally, diopside-plagioclase symplectite can be observed at omphacitic clinopyroxene grain boundaries and retrograde plagioclase surrounding quartz. c. Fine-grained mixture of omphacitic clinopyroxene, clinozoisite, quartz, minor amphibole and kyanite being replaced by retrograde plagioclase. Clinozoisite and kyanite show a shape preferred orientation. d. Banded inclusion-rich garnet aggregate adumbrating former coronitic structure. Garnet aggregates preferentially disaggregate perpendicular to the foliation. Nevertheless, inclusion trails can be traced through several garnet fragments. Separated fragments show an inclusion-free garnet rim.

The mineral composition in intermediate strain eclogite is similar to the one of low strain eclogite. Garnet shows minor chemical fluctuations and has an average composition of Xalm = 0.36, Xpyr = 0.41, Xgrs = 0.22 and Xsps = 0.01 (Fig. 5a). Clinopyroxene has mostly an omphacitic composition with a XNa ranging between 0.25 and 0.31, with an average of 0.28. Its XMg is comprised between 0.88 and 0.90. The composition is in general very homogeneous over single grains. Clinopyroxene in contact with the fgpa however shows minor chemical zoning in the form of a Ca increase and Na decrease along grain boundaries. Clinozoisite has the same chemical characteristics as in low strain eclogite. The composition of retrograde plagioclase varies between Xab = 0.70 and Xab = 0.77.
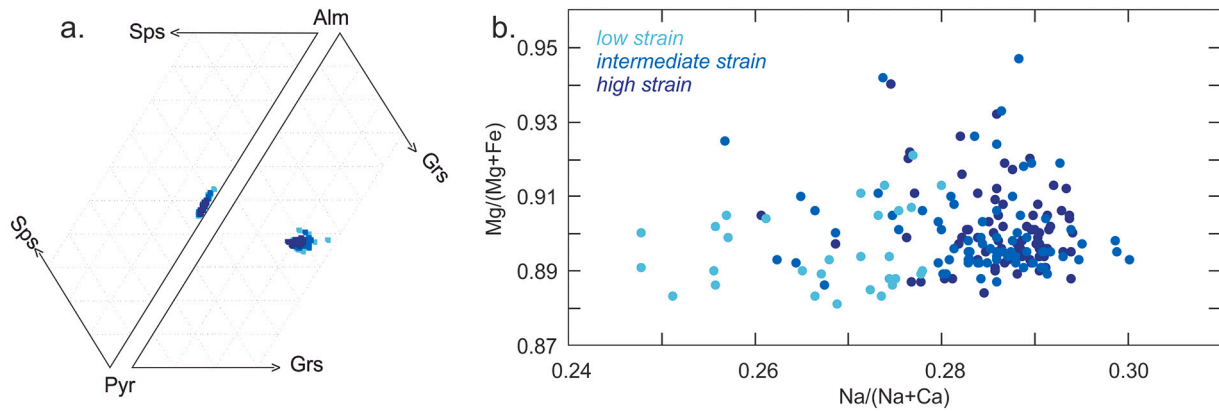
Fig. 5. Composition of garnet (a) and omphacitic clinopyroxene (b) in low strain (light blue), intermediate strain (blue) and high strain (dark blue) eclogite. Garnet and clinopyroxene composition get homogenized with strain. (For interpretation of the references to colour in this figure legend, the reader is referred to the web version of this article.)

4.1.3. High strain eclogite

High strain eclogite is characterized by a strong foliation defined by the clinopyroxene SPO (Fig. 3d), banded garnet aggregates (Fig. 4d) and intercalated thin foliation subparallel to parallel layers of fgpa with a strong SPO of all phases (Fig. 3d, e). As in intermediate strain eclogite, only large garnets with a size between 500 and 1000 μm are observed. Garnet aggregates dismember in a discontinuous manner preferentially along grain boundaries perpendicular to the foliation (Fig. 4d). Even though such aggregates clearly consist of polycrystalline garnet, it is possible to trace inclusion trails across entire dismembered aggregates (Fig. 4d). A thin inclusion-free garnet rim of approximately ~30 μm can always be observed next to zones of disaggregation. Again, preferred orientated crystals with long axes parallel to the extensional direction can be observed between dismembered garnet aggregates. Locally,
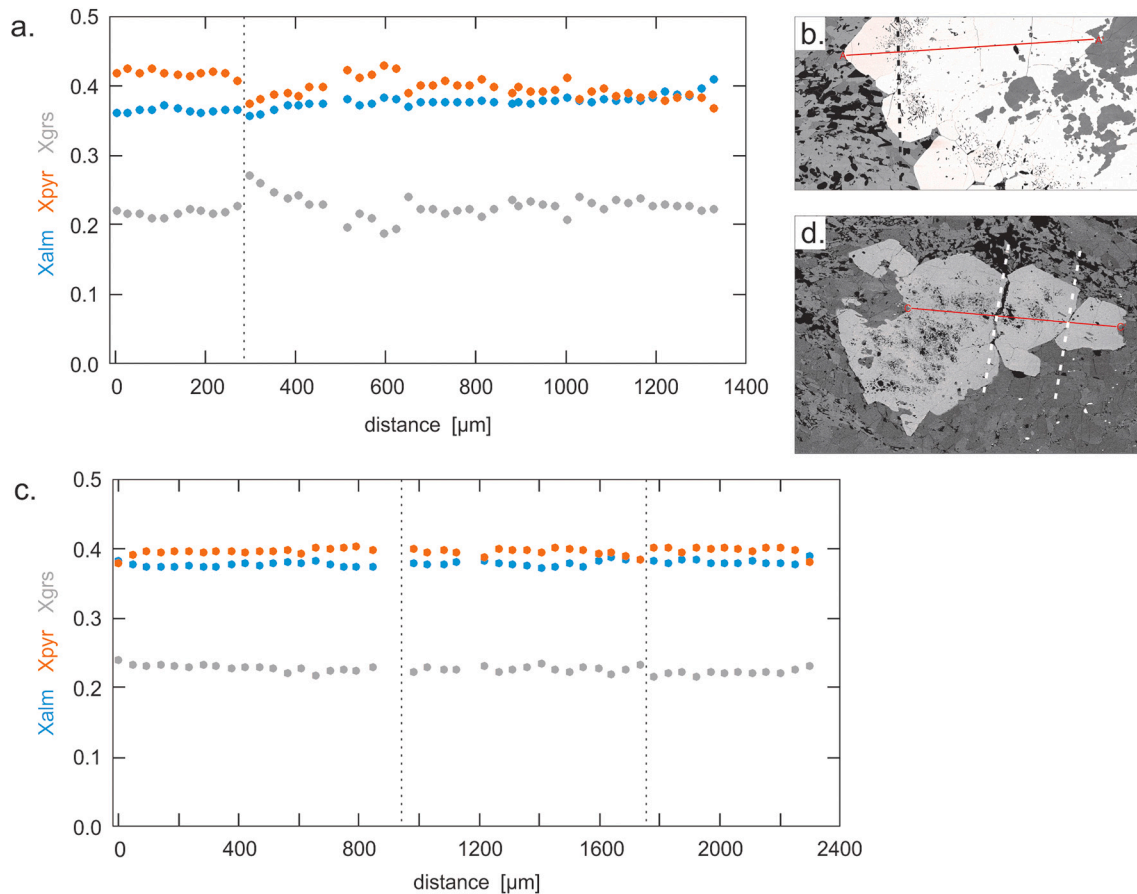

Fig. 6. a. Chemical composition profile across a polycrystalline garnet corona (red line in b) in a low strain eclogite. The black dashed line separates coarse grained garnet with crystal faces from fine grained garnet aggregate. b. Backscattered electrons image showing the position of the profile (red line). c. Chemical composition profile across disaggregating garnet aggregate in high strain eclogite (red line in d). Dotted lines represent locality of garnet disaggregation. d. Backscattered electrons image showing the position of the profile (red line). (For interpretation of the references to colour in this figure legend, the reader is referred to the web version of this article.)

garnet crystals entirely decoupled from the aggregates and fully surrounded by matrix clinopyroxene occur. In areas where garnet is particularly abundant the dominant foliation can be locally deflected.

The matrix clinopyroxene is only of type cpx2 (~50–300 μm) and has a significantly more intense SPO than in the intermediate strain eclogite. Its aspect ratio is slightly lower (average AR of 0.4, mode AR 0.39). Grain indentation can be observed along grain boundaries parallel to the foliation, with lobes orientated perpendicular to the foliation (Fig. 3f).
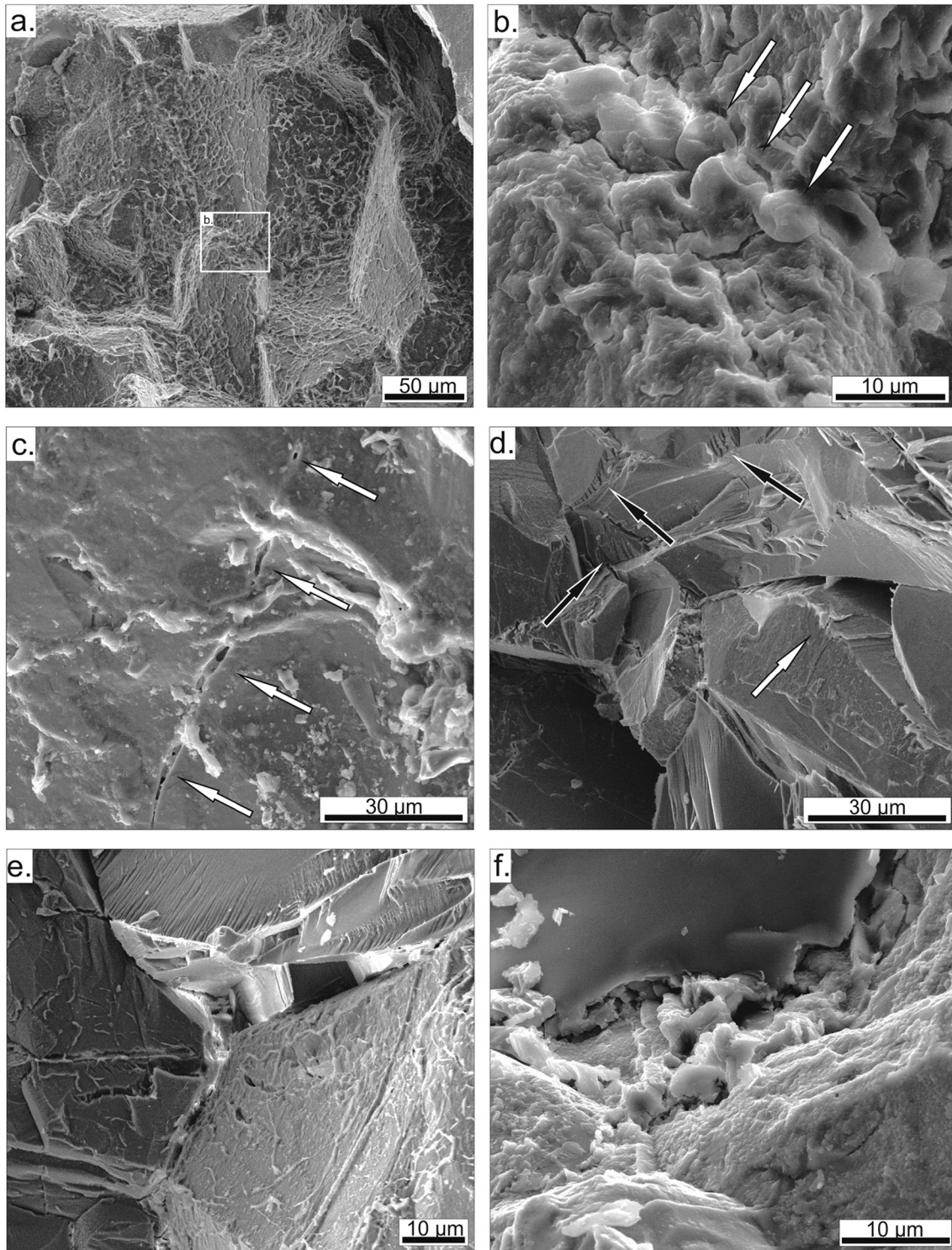
Fig. 7. Secondary electron images of broken surfaces of low strain eclogite. a. Vein like network of reprecipitate coating the garnet grain surface. The white rectangle marks close up shown in b. b. Close up of coating on garnet surface revealing small crystal nuclei on grain boundaries (white arrows). c. Garnet surface coated by reprecipitate. White arrows point on a partly sealed micro-crack. d. Rather smooth omphacitic clinopyroxene grain surfaces revealing open pores at grain triple junctions (white arrow). Feather like cracks are likely cause of sample preparation (black arrows). e. Vein like network of reprecipitate coating the omphacitic clinopyroxene grain surfaces. f. Rough omphacitic clinopyroxene surface and open grain boundary. The smooth surface in the upper left corner of the image is likely caused by preparation.

Clinopyroxene is crosscut by late cracks normal to the foliation, also crosscutting the surrounding symplectite (SF.4c, ST.1).

Garnet and clinopyroxene have the same average composition as in the intermediate strain eclogites (garnet: Xalm = 0.37, Xpyr = 0.41, Xgrs = 0.22, clinopyroxene: XNa = 0.28, XMg = 0.88–0.9) and are very homogeneous across single grains. In contrast to garnet aggregates in low strain eclogite, chemical zoning in garnets was not observed and chemical profiles are completely flat (Fig. 5a, 6c, d). Clinopyroxene in contact with the fgpa however shows minor Ca increase and Na decrease perpendicular to grain boundaries as seen by variation in grey value in BSE images (Fig. 4d). Clinozoisite has the same chemical characteristics as in less deformed samples. The albite content in plagioclase is slightly larger than in the low and intermediate strain eclogite and varies between 0.76 and 0.81 (Table 1).

4.2. Grain surface characteristics

Secondary electron images of broken sample surfaces from low strain eclogite samples show that the minerals often have a rough surface coated by a fine grained material (Fig. 7). Locally, the coating developed a vein like network with a vein width of a few microns. The density of the network is highly variable (Fig. 7a, e). Characterizing the chemistry of this material is beyond the scope of this study. Up to 5 μm garnet crystals locally nucleated within this coating (Fig. 7b). Rare micro-cracks within garnet up to 5 μm in width are partly filled with the same material coating garnet (Fig. 7c). While a similar coating can be observed on garnet and clinopyroxene crystals in areas with a heterogeneous phase-size distribution, it appears that mono-phase areas with a homogeneous grain-size distribution are characterized by rather smooth surfaces (Fig. 7d). However, those areas locally preserve open grain boundaries that are partly sealed by reprecipitate (Fig. 7f). Additionally, angular cavities at grain triple junctions occur in cpx2 dominated areas (Fig. 7d).

In contrast, deformed eclogite show relatively smooth clinopyroxene and garnet grain surfaces (Fig. 8). The rock fabric seems compact and secondary electron images do not reveal any open grain boundaries or cavities. Only in symplectite rich areas grain boundaries and triple junctions are partly sealed by fine grained material, likely cpx3 diopsidic clinopyroxene and plagioclase (Fig. 8a). Despite the compact nature of the rock fabric, a similar reprecipitate to ones in the low strain eclogite can be observed. However, the rough topography and vein like network are lacking here (Fig. 8b).

4.3. Crystallographic orientation and intracrystalline distortion

Stereographic projections of [001] axis and poles to (010) and (100) of omphacitic clinopyroxene from the low strain eclogite do show several single maxima. However, the distribution of those maxima appears rather random when compared to documented omphacite textures (Fig. 9a; Keppler, 2018 and references therein). With increasing strain, the orientation of omphacitic clinopyroxene is changing and the CPO progressively changes. Crystals from intermediate strain eclogite show a slightly preferred alignment of [001] axes orientated on a girdle sub-parallel to parallel to the foliation and (010) poles sub-perpendicular to the foliation (Fig. 9b). In high strain eclogite omphacitic clinopyroxene shows a similar CPO to the one in intermediate strain eclogite though more pronounced. The (010) point maxima are perpendicular to the foliation and [001] axes define a girdle within the foliation (Fig. 9c). These characteristics are similar to the S-type CPO of omphacite (Helmstaedt et al., 1972). Despite the development of a CPO, we do not observe indication of intracrystalline plasticity in omphacitic clinopyroxene. Grain-average orientation maps reveal that the average misorientation in strained eclogite is overall below 1.8 (Fig. 10a, b). Data from EBSD mapping are in agreement with the lack of undulatory extinction or abundant low-angle grain boundaries.

Garnet from all localities has a random crystallographic orientation. Polycrystalline aggregates (Fig. 10c, d) in corona structures as well as garnet from stretched disaggregated aggregates (Fig. 10e, f) are composed of crystals with varying orientations. Nevertheless, coronitic garnet shows a heterogeneously dispersed intracrystalline misorientation that increases towards the corona center (Fig. 10d). In the intermediate to high strain eclogite samples garnet crystals show minor intracrystalline misorientation with misorientation angles up to 5° across single grains (Fig. 10f). Misorientation profiles reveal local jumps up to 2.8° which might originate from arranged dislocation walls or late micro-cracking (Fig. 10g).

4.4. Thermodynamic forward modeling

The pressure-temperature conditions and H$_2$O activity that are recorded in the investigated samples described above were estimated using thermodynamic forward modeling (see Section 3.2 for detail on the methods). Petrographic observations suggest that the eclogitic equilibrium assemblage is composed of garnet, omphacitic clinopyroxene, clinozoisite, kyanite, quartz and rutile. The occurrence of clinozoisite indicates that H$_2$O was present in the system during
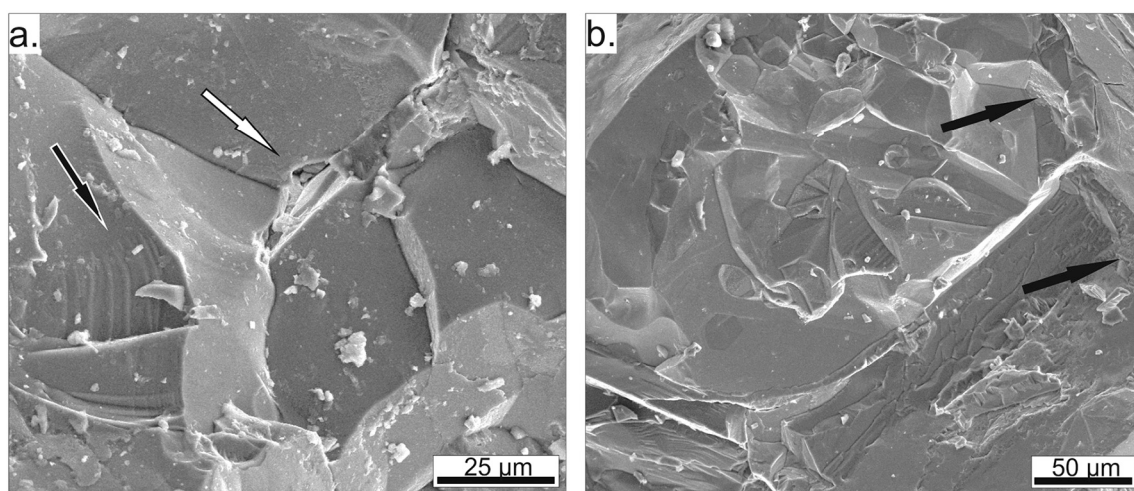

Fig. 8. Secondary electron images of broken surfaces of high strain eclogite. a. Smooth omphacitic clinopyroxene grain surfaces with straight grain boundaries. Small, partly filled pores occur at grain triple junctions (white arrow). b. Grain network without any porosity or open grain boundaries. Crystal surfaces are rather smooth with minor sides of reprecipitate (black arrows).
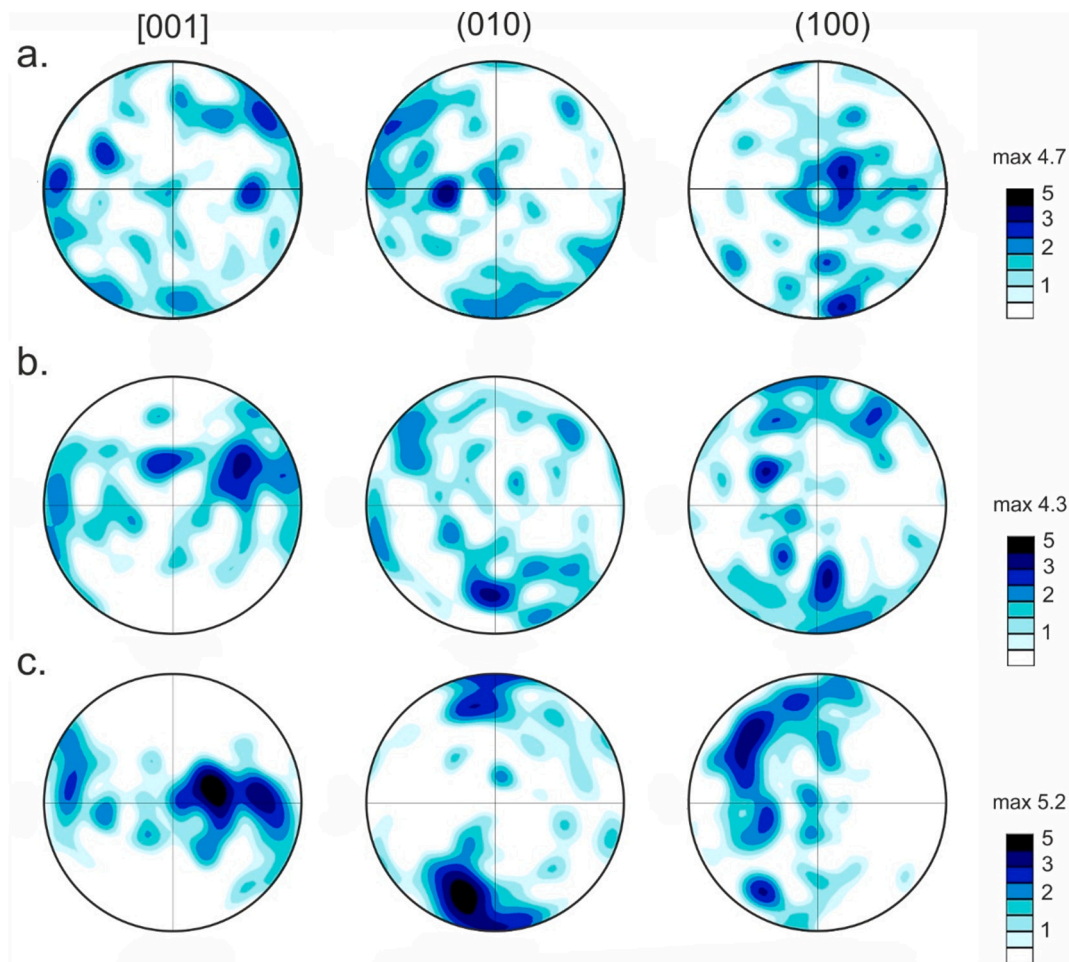
Fig. 9. Stereographic projection of [001] axis, (010) and (100) poles of omphacitic clinopyroxene in low strain (a), intermediate strain (b) and high strain (c) eclogite. Equal area, upper hemisphere projection. a. close to random crystallographic orientation of omphacitic clinopyroxene in the matrix of coronitic eclogite. (100) poles are orientated preferentially parallel to Y (pole figure center) while (010) poles form a very dispersed girdle sub-normal to the foliation. [001] axes do not show any preferred alignment. Number of analyzed grains: 736. b. preferred alignment of [001] axes forming a girdle approximately parallel to the foliation. Poles to (100) and (010) planes are aligned on a dispersed girdle normal to sub-normal to the foliation. Number of analyzed grains: 332. c. [001] axes are aligned on a girdle parallel to the foliation while poles to [010] show a point maximum perpendicular to the foliation. Number of analyzed grains: 908.

eclogitization and subsequent deformation at eclogite facies conditions. Amphibole is subordinate and it is unclear if it belongs to the eclogitic assemblage. The average compositions of unzoned garnet (XFe = 0.37, XMg = 0.40, XCa = 0.23) and omphacitic clinopyroxene (XNa = 0.27, XMg = 0.88) barely change with the intensity of strain (Figs. 5 and 6) and are representative for the three degrees of strain. These values are considered for the chemical tests.

Calculations considering all phases in the database (Fig. 11a, b) show that the inferred equilibrium assemblage (field label: Grt Czo Ky Qtz Rt in bold) is stable for a wide range of P-T-a(H$_2$O) conditions. The corresponding field is bounded at low pressure by the amphibole-in reaction, which is almost superimposed with the kyanite-out reaction, at high pressure by the quartz-coesite transition, at low temperature by a set of lawsonite-in reactions and at low H$_2$O activity by the quartz-out and clinozoisite-out reactions. The results of the chemical tests on garnet and clinopyroxene tests are represented as coloured background of Fig. 11a, b. The blue and yellow backgrounds correspond to 0 and 5 positive tests, respectively. The chemical fit is rather poor in the whole P-T-a(H$_2$O), even if a large tolerance of 0.05 is used for the tests. The five tests are positive only in fields where lawsonite is stable, for $P > 2.6$ GPa and a (H$_2$O) > 0.95. These conditions are close to the coesite stability field and are considered as unrealistic for the following reason. In the field where lawsonite is stable, quartz, kyanite and clinozoisite are predicted to be absent. If lawsonite would be a prograde phase, this would be

incompatible with the occurrence of quartz, kyanite and clinozoisite as inclusions in garnet coronae, which correspond to the earliest microstructures that we could identify.

A range of conditions with only four positive tests occurs between the field corresponding to the inferred equilibrium assemblage (field label: Grt Czo Ky Qtz Rt in bold) at high pressure and a field where an amphibole is stable instead of kyanite (field label: Grt Czo Amp Qtz Rt) at lower pressure. It is located around 680 °C and 2.3 GPa and corresponds to rather high a(H$_2$O) > 0.7. The closest chemical fit is achieved for 670 °C-2.35 GPa and unit H$_2$O activity. However, the predicted garnet composition is systematically too rich in Ca (XCa > 0.29). Examination of the XCa isopleths in garnet shows that they mostly depend on pressure and H$_2$O activity. They decrease in a concentric manner in the direction of the amphibole-in and kyanite-out reactions. The effect of a(H$_2$O) on the XCa isopleth in the Grt Czo Ky Qtz Rt stability field is related to the reaction.

4 grossular (Grt) + 5 Ky + Qtz + 3 H$_2$O = 6 clinozoisite (Czo), (1)
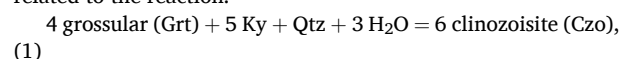
which promotes the formation of clinozoisite at the expense of grossular as a(H$_2$O) increases. These observations suggest that garnet with a Ca-poorer composition similar to the measured one might be predicted in absence of amphibole. It would also imply that the predicted amphibole stability field is too large at high pressure.

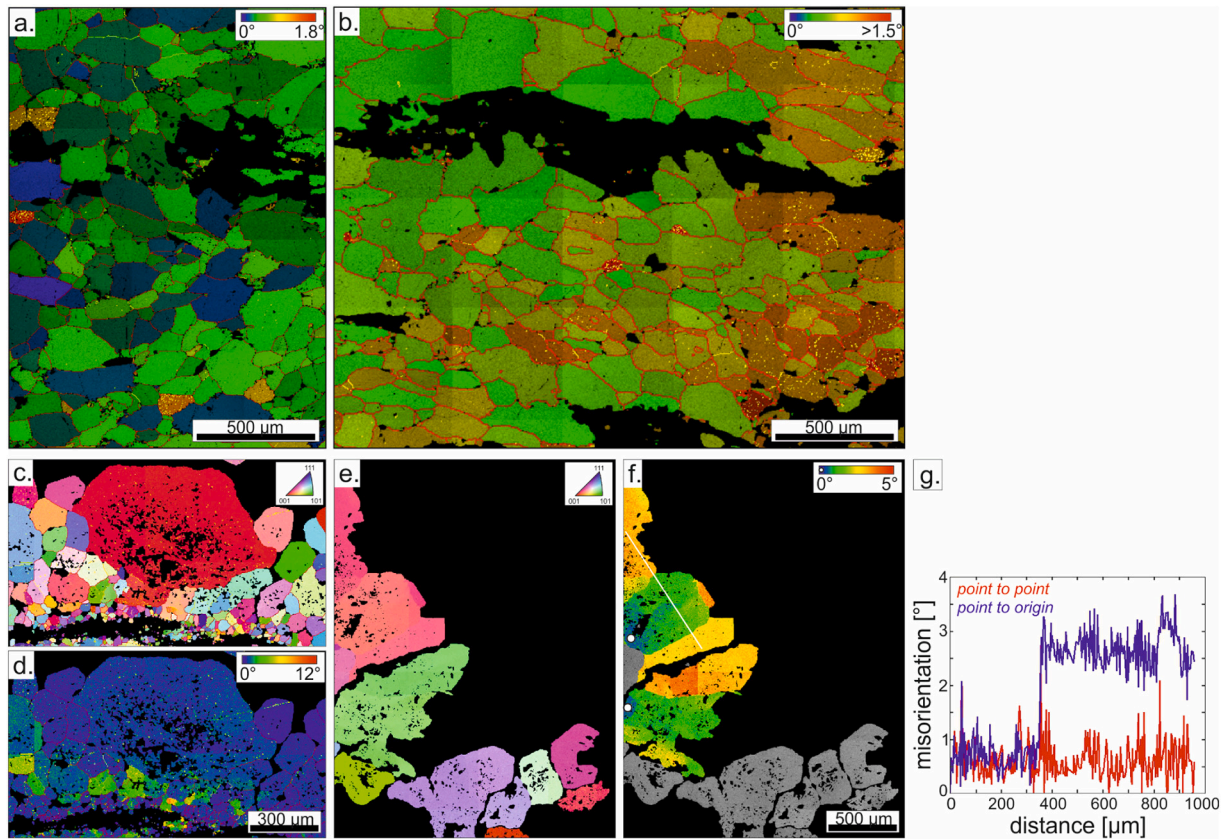In order to test this hypothesis, we carried out the same calculations,

Fig. 10. a. Grain-average orientation map of omphacitic clinopyroxene from intermediate strain eclogite revealing that the crystal lattice is almost unstrained. High-angle grain boundaries (>10°) are coloured in red, low-angle grain boundaries (3–10°) in yellow. b. Grain-average orientation map of omphacitic clinopyroxene from high strain eclogite showing a strong SPO while the crystal lattice is almost unstrained. Only very few subgrains occur. High-angle grain boundaries (>10°) are coloured in red, low-angle grain boundaries (3–10°) in yellow. c. Electron-backscatter diffraction map of coronitic garnet in low strain eclogite. Colour-code according to inverse pole figure. High-angle grain boundaries (>10°) are coloured in red, low-angle grain boundaries (3–10°) in yellow. Note the random crystallographic orientation of grains and the decrease in grain size towards the corona center (lower part of the panel). d. Misorientation deviation angle map revealing an increased misorientation deviation in garnet grains towards the corona center (lower part of the panel). High-angle grain boundaries (>10°) are coloured in red, low-angle grain boundaries (3–10°) in yellow. e. Electron-backscatter diffraction map of partly disaggregated garnet aggregate in intermediate strain eclogite. Colour-code according to inverse pole figure. Note that garnet grains preferentially detach along grain boundaries. f. Image quality map with overlying colour coding displaying the relative misorientation to a single point (white dot) across two grains. The white line represents the position of misorientation profile shown in e. g. Misorientation profile across a garnet grain. The point-to-point (red) as well as point-to-origin curves show two large misorientation jumps at about 390 μm and 810 μm. (For interpretation of the references to colour in this figure legend, the reader is referred to the web version of this article.)

discarding the amphibole model from the thermodynamic database. The results are presented on a P-T diagram for a(H_2O) = 1 (Fig. 11c) and a P-a(H_2O) diagram for T = 640 °C (Fig. 11d). In absence of amphibole, the Grt Czo Ky Qtz Rt stability field is extended to lower pressure and the decrease in pressure below ~2.1 GPa induces a decrease in Ca content of garnet in agreement with the measured composition. Hence, the five chemical tests are positive for T ~ 640 °C, P = 1.9–2.0 GPa and a(H_2O) > 0.95, even with a reduced tolerance of 0.005. These conditions fall within the stability field of the inferred equilibrium assemblage (Cpx Grt Czo Ky Qtz Rt in bold). For other conditions the composition of garnet and clinopyroxene changes rapidly and does not match anymore the measured one.

5. Discussion

Microstructural and petrological investigations provide crucial information on the evolution of fluid pathways and the role of H_2O during the formation and deformation of the Al-Mg-rich eclogite from the outcrop of Hohl. These aspects and their implications are discussed here.

5.1. Evidence for a H_2O dominated fluid phase at eclogite peak conditions

Depending on the validity of the thermodynamic data and activity model of amphibole, two conclusions are possible. On the one hand, if the amphibole model is considered, the measured chemical composition of garnet and clinopyroxene is rather poorly reproduced, with the best match being reached around T = 670 °C, P = 2.35 GPa and a(H_2O) > 0.7, probably close to 1. At those conditions either kyanite at high pressure or amphibole at low pressure is stable, with a very narrow range of conditions where both are stable. On the other hand, if the amphibole model is discarded, the measured chemical composition of garnet and clinopyroxene is close to perfectly reproduced around T = 640 °C, P = 1.9–2.0 GPa and a(H_2O) > 0.95. At these conditions, the stable assemblage corresponds to the inferred one. This is our favored interpretation. Irrespective of the conclusion, there is a strong contrast between the variability of composition (especially in garnet) as shown by the densely spaced isopleths and the chemical homogeneity of the phases in the investigated samples. This indicates that the eclogite almost fully equilibrated at the conditions of metamorphism and deformation.

Issues related to amphibole overstability is not surprising since the amphibole model has been developed for pressure lower than those
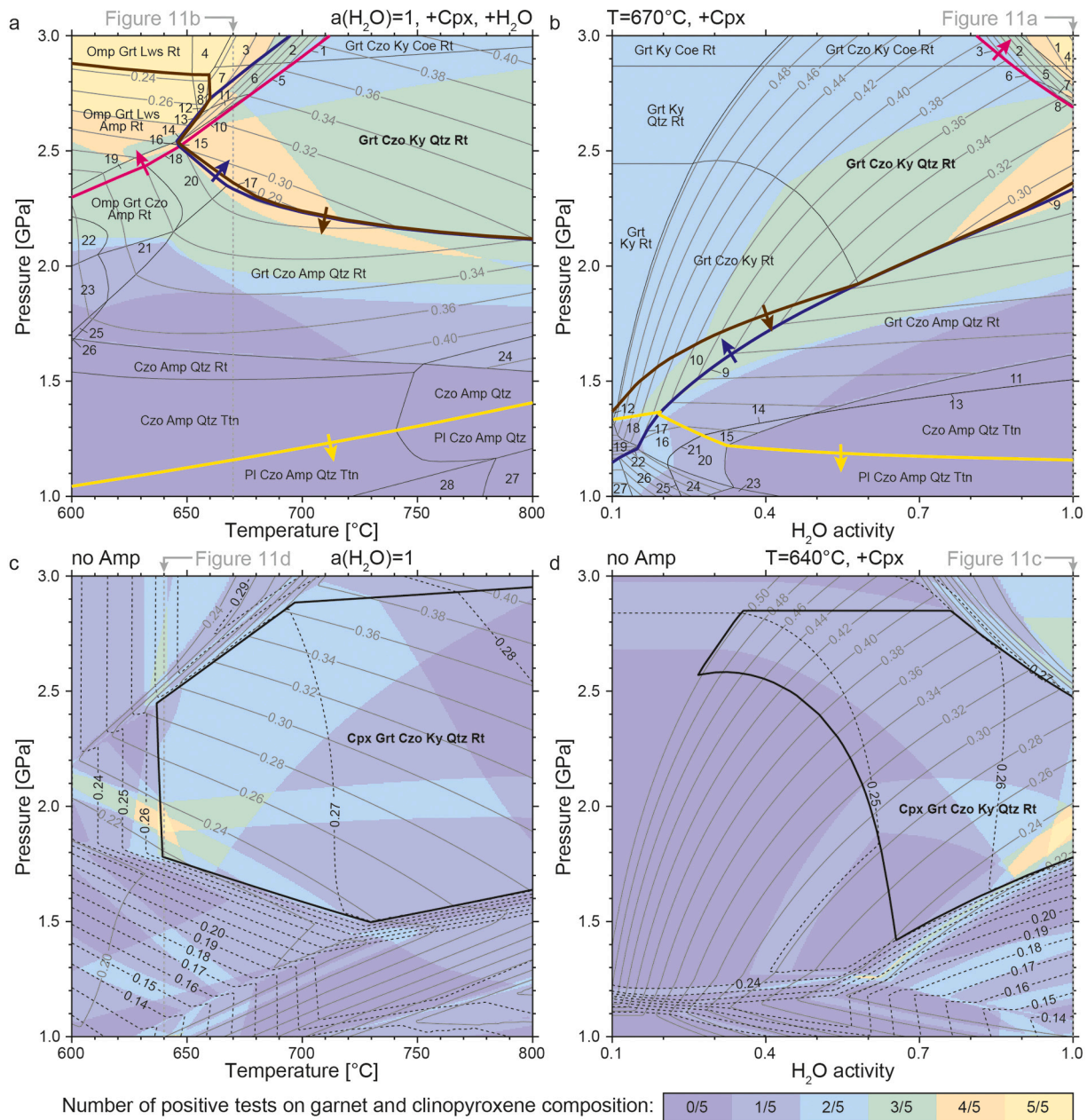
Fig. 11. Pseudosections calculated for the average eclogitic Al-Mg-rich metagabbro composition (see Section 3.2 for detail). The coloured background indicates the number of positive chemical tests, considering a tolerance of 0.05 (a, b) and 0.005 (c, d). Solid grey lines: isopleths of XCa in garnet, dashed black line: isopleths of XNa in clinopyroxene. a. Pressure-Temperature pseudosection calculated with a(H$_2$O) = 1 (i.e. excess H$_2$O). H$_2$O and a disordered clinopyroxene (omphacitic at high pressure and calcic at low pressure) are stable in all fields. The assemblage of numbered fields are 1: Grt Czo Lws Ky Coe Rt, 2: Grt Lws Ky Coe Rt, 3: Grt Lws Coe Rt, 4: Grt Lws Rt, 5: Grt Czo Lws Ky Qtz Rt, 6: Grt Lws Ky Qtz Rt, 7: Grt Lws Qtz Rt, 8: Grt Lws Amp Qtz Rt, 9: Grt Lws Amp Rt, 10: Grt Czo Lws Ky Rt, 11: Grt Lws Ky Rt, 12: Grt Lws Ky Amp Qtz Rt, 13: Grt Lws Amp Ky Rt, 14: Omp Grt Lws Amp Ky Rt, 15: Grt Czo Lws Amp Ky Qtz Rt, 16: Omp Grt Czo Lws Amp Ky Rt, 17: Grt Czo Amp Ky Qtz Rt, 18: Omp Grt Czo Lws Amp Qtz Rt, 19: Omp Grt Czo Lws Amp Rt, 20: Omp Grt Czo Amp Qtz Rt, 21: Grt Czo Amp Rt, 22: Omp Grt Czo Amp Gln Rt, 23: Grt Czo Amp Gln Rt, 24: Grt Czo Amp Qtz, 25: Grt Czo Amp Gln Qtz Rt, 26: Czo Amp Gln Qtz Rt, 27: Pl Amp Qtz, 28: Pl Amp Qtz Ttn. The lawsonite-in, kyanite-in, amphibole-in and plagioclase-in reactions are indicated by thick pink, dark blue, brown and yellow lines, repectively. The arrow points into the stability field of the considered mineral. b. Pressure-H$_2$O activity pseudosection calculated at 670 °C. A disordered clinopyroxene (sodic at high pressure and calcic at low pressure) is stable in all fields. The assemblage of numbered field is 1: Grt Lws Coe Rt, 2: Grt Lws Ky Coe Rt, 3: Grt Czo Lws Ky Coe Rt, 4: Grt Lws Qtz Rt, 5: Grt Lws Ky Qtz Rt, 6: Grt Czo Lws Ky Qtz Rt, 7: Grt Lws Ky Rt, 8: Grt Czo Lws Ky Rt, 9: Grt Czo Amp Ky Qtz Rt, 10: Grt Czo Amp Ky Rt, 11: Czo Amp Qtz Rt, 12: Grt Amp Ky Rt, 13: Czo Amp Qtz Rt Ttn, 14: Grt Czo Amp Qtz Rt Ttn, 15: Grt Czo Amp Qtz Ttn, 16: Grt Pl Czo Amp Qtz Rt, 17: Grt Pl Czo Amp Ky Qtz Rt, 18: Grt Pl Czo Amp Ky Rt, 19: Grt Pl Amp Ky Rt, 20: Grt Pl Czo Amp Qtz Ttn, 21: Grt Pl Ep Amp Qtz Rt Ttn, 22: Grt Pl Amp Ky Qtz Rt, 23: Pl Amp Qtz Ttn, 24: Grt Pl Amp Qtz Ttn, 25: Grt Pl Amp Qtz Rt Ttn, 26: Grt Pl Amp Qtz Rt, 27: Grt Pl Amp Rt. The lawsonite-in, kyanite-in, amphibole-in and plagioclase-in reactions are indicated by thick pink, dark blue, brown and yellow lines, repectively. The arrow points into the stability field of the considered mineral. c. Pressure-Temperature pseudosection calculated with a(H$_2$O) = 1 (i.e. excess H$_2$O) by discarding the amphibole model from the database. Only the boundaries of the field corresponding to the inferred equilibrium assemblage are shown. d. Pressure-H$_2$O activity pseudosection calculated at 640 °C by discarding the amphibole model from the database. Only the boundaries of the field corresponding to the inferred equilibrium assemblage are shown. Mineral abbreviations after Whitney and Evans (2010). (For interpretation of the references to colour in this figure legend, the reader is referred to the web version of this article.)

considered here and should be applied with care at pressure larger than 2 GPa (Green et al., 2016). The model also tends to incorporate Al in excess, which might exaggerate the stability of amphibole in the considered Al-rich chemistry. We are fully aware that conditions determined by discarding amphibole from the thermodynamic database and, at the same time, using only equilibrium assemblages might be wrong. However, we are confident that our approach is legitimate since the conditions are determined also considering the phase chemistry of garnet and clinopyroxene and the amount of amphibole observed in the investigated samples is negligible.

Minimal uncertainties of 0.1 GPa on pressure and 30 °C on temperature should be applied to the P-T estimates (Plunder et al., 2012). Considering these uncertainties, the temperature of eclogitization determined here (640 °C) is compatible with previous estimates of the eclogite peak (Miller et al., 2007; Bruand et al., 2010; Schorn and Diener, 2017; Schorn, 2018). The favored low-pressure estimate (1.9–2.0 GPa) is similar within the uncertainties to the peak estimate of 1.85 GPa (Bruand et al., 2010) determined in eclogite of different chemistry (Fe-Ti-rich metagabbro) for the same outcrop of Hohl. This agreement and the excellent match of garnet and clinopyroxene compositions suggests that the conditions T = 640 °C, P = 1.9–2.0 GPa and a (H_2O) > 0.95 are more representative of the eclogitization. Notice however that in both cases the chemical assemblage and the composition of garnet and clinopyroxene point to an H_2O activity close to one and, in any case, larger than 0.7. A high H_2O activity or even pure H_2O saturation at eclogite facies conditions has already been proposed for the eclogites of the SKC based on study of natural samples (Bruand et al., 2010; Schorn and Diener, 2017). An experimental study on eclogitization of gabbro from the SKC also suggested the presence of a free fluid phase during eclogitization (Tropper et al., 2008). It however inferred that the fluid was not pure H_2O and might have contained 30% NaCl. The source of fluid assisting the eclogization has be proposed to be the surrounding metasediment that dehydrate at eclogite facies conditions (Schorn, 2018). This study suggests that gabbro paragenesis was metastable up to eclogite facies conditions until the released fluids acted as catalyst for the metamorphic reactions, triggering the replacement of the metastable gabbro by eclogite. We therefore conclude that eclogitization and subsequent deformation under the influence of a H_2O dominated fluid occurred at peak conditions characterized by T = 640 °C, P = 1.9–2.0 GPa and a(H_2O) > 0.95.

5.2. Eclogitization by dissolution-precipitation

In agreement with previous studies on eclogites of the type locality (Bruand et al., 2010; Schorn and Diener, 2017; Schorn, 2018) and of other occurrences (Austrheim, 1987; Jamtveit et al., 1990; Pennacchioni, 1996; Engvik et al., 2001; John and Schenk, 2003; Austrheim, 2013; Zertani et al., 2019), our study emphasizes the presence of a fluid phase during eclogitization. Even though the typical eclogite mineral assemblage is dominated by nominally water free phases (garnet, omphacitic clinopyroxene), H_2O is needed to transform a dry metastable protolith (gabbro, mafic granulite) into an eclogite that is stable at high-pressure conditions during orogeny (Austrheim, 2013 and references therein). Our observations however provide new insights in the mechanisms of mass transfer active during this transformation, and especially on the role of dissolution-precipitation.

Field and microstructural observations suggest that coronitic eclogite represents an initial stage of eclogitization in the SKC. These low strain eclogites are characterized by a coronitic fabric where garnet coronae have grown at the interface between magmatic plagioclase and clinopyroxene, and locally mimic the former gabbroic fabric (Proyer and Postl, 2010; Schorn and Diener, 2017). The internal structure of the garnet coronae is characterized by coarse crystal faces towards the outer side corresponding to magmatic plagioclase partly replaced by fine grain aggregate of clinozoisite, kyanite and quartz and fine grained intergrowths of garnet, clinopyroxene and minor quartz towards the

center corresponding to magmatic clinopyroxene. Such a contrast in garnet morphology is usually interpreted by preferential growth of garnet towards plagioclase (Mørk, 1985). Nevertheless, the similar chemical composition measured at both ends of the chemical profiles of garnet coronae indicates that garnet grew in both directions. Different microstructures at both ends of the garnet coronae suggest that two different processes could have been co-active. On the one hand, large crystal faces towards the outer side of the coronae likely occurred by continuous garnet growth of a single crystal. On the other hand, fine grained intergrowth of garnet and clinopyroxene towards the corona center indicate a high nucleation rate of new small garnet and clinopyroxene crystals (Mullin, 2001). The smooth decrease of grossular content towards the inside of the corona (Fig. 6a) would then indicate that nucleation of small garnet crystals at the onset of eclogitization was more efficient than single crystal growth, whereas the observed mineral chemistry at both ends of the garnet coronae profiles point to formation at peak conditions. The mineral replacement of magmatic (and probably cpx1) clinopyroxene and plagioclase by monoclinic cpx2 omphacitic clinopyroxene and cubic garnet results in non-epitactic growth, which is known to promote nucleation of a polycrystalline or even polyphase material instead of a continuous reaction front (Putnis and Putnis, 2007).

Irrespective of the processes forming the complex coronae, the development of a polycrystalline material results in an increase of grain boundary density, which can enhance diffusion and subsequent metamorphic reactions in two possible ways. Firstly, grain and phase boundaries act as high-diffusion pathways for element diffusion without the support of any fluid (Keller et al., 2006, 2008; Gardés et al., 2011). Secondly, grain and phase boundaries can act as preferred pathways for fluids supporting mineral replacement (Milke et al., 2007; Gardés et al., 2012). The step in chemical profile towards the outer coronae rim indicates that volume diffusion was a rather subordinate process, too inefficient to smoothen the chemical profile. In contrast, dihedral angle traced by the vein-like network coating garnet grain boundaries suggests that grain boundaries were fluid saturated (Mancktelow et al., 1998). This is consistent with the estimated H_2O activity close to 1. It is therefore likely that mass transfer related to eclogitization was assisted by a fluid phase dominated by H_2O saturating the grain and phase boundaries.

Microstructures observed in the low strain eclogite, including partly rough grain boundary surfaces and vein like coating raise the hypothesis that dissolution-precipitation was active (Mancktelow et al., 1998; Menegon et al., 2008). In this framework, the coating is interpreted as precipitate tracing dihedral angles along grain boundaries and triple-junctions. The rather smooth surface of garnet crystals on these precipitate additionally suggests that crystals nucleated in H_2O saturated conditions (Menegon et al., 2008). No unambiguous evidence for dissolution could be observed in low strain eclogite. This is actually perfectly consistent with full dissolution of the gabbro phases that were metastable at eclogite facies conditions.

5.3. Deformation of eclogite by dissolution-reprecipitation creep

The macroscopic changes from low strain coronitic to high strain foliated eclogite is accompanied by several microstructural changes that are likely linked to strain accommodation and discussed in the following in the general frame of deformation at eclogite facies conditions. Though dismembered garnet coronae do show minor indication of brittle deformation in the form of micro-cracks, the overall deformation behaviour of the investigated samples is ductile. Cracks observed in omphacitic clinopyroxene grains in foliated eclogites are a post-eclogitic feature as they crosscut elongated grains and their surrounding symplectite.

Almost identical mineral compositions in all three sample sets together with the growth of peak metamorphic minerals in dilation sites between grains of dismembering garnet aggregates indicate that

eclogitization and deformation of the eclogite occurred at nearly stable conditions at the metamorphic peak or close to it. The most striking changes with progressive strain are the development of a pronounced foliation characterized by a CPO and a strong SPO of omphacitic clinopyroxene as well as the flattening and elongation of garnet coronae.

The clinopyroxene SPO increases progressively, as reflected by the decreasing grain aspect ratio. In parallel omphacitic clinopyroxene develops a texture which has the same characteristics as the S-type CPO of omphacite (Helmstaedt et al., 1972). These microstructural features are often associated with crystal plastic deformation, or more specific dislocation glide (Buatier et al., 1991; Bascou et al., 2001, 2002; Kurz et al., 2004; Zhang et al., 2006; Moghadam et al., 2010). However, the omphacitic clinopyroxene in the investigated foliated eclogite hardly reveals any positive evidence of crystal plasticity like undulatory extinction, subgrains or sutured grain boundaries. Additionally, EBSD maps show that grain average misorientation usually lies below 2°. We therefore argue that omphacitic clinopyroxene deformed rather by diffusion and/or dissolution-precipitation creep. The strong anisotropy of clinopyroxene is known to result in diffusion rates one order of magnitude higher along [001] than in other crystallographic directions, likely resulting in a preferred alignment of [001] parallel to the lineation (Mauler et al., 2001). Preferred dissolution of clinopyroxene grains having [001] perpendicular to the foliation and (010) parallel to the lineation in conjunction with fast growth of grains with [001] parallel to the lineation and (010) perpendicular to the foliation can explain the strengthening of the S-type CPO with strain. Foliation parallel preferred alignment of omphacitic clinopyroxene in dilation sites (e.g. between decoupling garnet grains) and indentation between grains supports the hypothesis that clinopyroxene deformed dominantly by dissolution-reprecipitation creep (Wassmann and Stöckhert, 2013) assisted by minor diffusion creep (Mauler et al., 2001).

In parallel to deformation of omphacitic clinopyroxene, the garnet coronae formed during eclogitization flatten and stretch, forming aggregates sub-parallel to the foliation. The rearrangement of garnet aggregates during strain accommodation is accompanied by a homogenization in grain size at the expense of the small grain fractions, which might be explained by various processes. The initially heterogeneous grain size distribution of coronitic garnet and high density of small grains results in a high surface energy of the system, which might be the driving force for grain coarsening via Ostwald ripening (Ostwald, 1900; Griggs et al., 1960).

The mass transfer driven by reduction of surface area and resulting energy in the system can either occur by volume diffusion (Ostwald, 1900; Martin et al., 1997) or dissolution-reprecipitation (Martin et al., 1997). Nevertheless, the surface energy of a system is in general a rather small factor, which is only responsible for microstructural changes if other energies are low. Here the development of the foliation clearly indicates a dynamic system in which strain accommodation played a crucial role. Therefore, the observed microstructural changes are likely the result of combined processes resulting in surface energy reduction and strain accommodation. Previous studies have shown that crystals with a higher dislocation density tend to have a higher dissolution rate (Wintsch, 1980; Schott et al., 1989). We hence suggest that in the course of flattening and extension of garnet coronae, the smaller garnet grains with a higher dislocation density from the coronae center (Fig. 10d) were dissolved and reprecipitated at larger garnet crystals, resulting in grain coarsening and concurrent reduction in strain and surface energy. Additionally, the occurrence of decoupled garnet crystals from aggregates indicates that garnet partly behaved as a rigid body in a weaker matrix. EBSD maps reveal that intracrystalline plasticity was a rather subordinate mechanism since coronae and flattened garnet aggregates are composed of randomly orientated, almost strain free crystals. Minor intracrystalline distortion observed at garnet-garnet contacts is likely resulting from local stress concentration.

Even though the present study focusses on the two main constituents of the investigated samples (omphacitic clinopyroxene and garnet), we briefly suggest possible deformation mechanisms for the fine grained polyphase aggregate of clinozoisite, kyanite and quartz (fgpa) during rearrangement into foliation subparallel layers. The polyphase nature of the fgpa is likely inhibiting grain growth by pinning of grain boundaries at second phases (Evans et al., 2001; Taska et al., 2017). Thus the homogeneous fine grain size promotes the activation of grain size sensitive mechanisms like diffusion creep, grain and phase boundary sliding (GBS and PBS), which are known to be more efficient in the accommodation of strain (Gifkins, 1976; Warren and Hirth, 2006; Zhao et al., 2019). High density in phase boundaries has been suggested to enhance boundary diffusion (Zhao et al., 2019). Additional presence of fluids as in the investigated samples might further increase diffusion processes (Milke et al., 2007). Once connected in subparallel layers it is likely that deformation of the fine grained polyphase aggregate by PBS accommodated significant amounts of the strain.

Microstructural and chemical observations of foliated eclogite reveal that the dominant mechanism active during the development of foliation was dissolution-reprecipitation accompanied by diffusion creep, at least in both garnet and omphacitic clinopyroxene. Subordinate dislocation creep and rigid body rotation in garnet as well as phase boundary sliding in the fine grained polyphase aggregate was co-active.

5.4. Evolution of fluid pathways at Hohl

Even though the classical eclogite assemblage consists of the non-hydrous minerals garnet and omphacite it is widely accepted that the transformation of a dry mafic protolith into an eclogite requires fluid infiltration (Austrheim, 1987; Pennacchioni, 1996; Austrheim et al., 1997; John and Schenk, 2003; Jolivet et al., 2005; Engvik et al., 2007; Cao et al., 2020). While the importance of fluids for eclogitization to occur is well established, the pathways by which they infiltrate the dry rock are variable and highly depend on whether mineral replacement occurs under static or dynamic conditions. Various studies have observed a positive feedback between deformation and introduction of fluid pathways either by micro-fracturing (Austrheim, 1987; Jamtveit et al., 1990; Engvik et al., 2007) or the activation of creep cavitation (Fusseis et al., 2009; Gilgannon et al., 2017).

Contrary to studies mentioned above our data rather indicate a reduction in fluid pathways with strain. In the low strained rocks, our data show that the replacement of coarse grained magmatic fabric with the finer grained metamorphic mineral assemblage resulted in an increased grain boundary density serving as fluid pathways in accordance with observed open grain boundaries and precipitate on crystal surfaces (Fig. 7). The occurrence of eclogite facies mineral nuclei within those precipitate and lack of retrograde phases is further strengthening the interpretation that those fluid pathways were active at eclogite facies conditions. Additionally, calculations with Theriak-Domino yield a density of 3.00 g/cm^3 for the gabbro protolith (dry average bulk at 1000 °C–0.25 GPa, Miller and Thöni, 1997) and 3.43 g/cm^3 for the eclogite (H$_2$O-saturated average bulk at 640 °C–1.95 GPa). Eclogitization of the metastable gabbro induced a corresponding volume reduction of about 14% and resulted in the development of a porosity at peak metamorphic conditions. These developing connected fluid pathways in turn facilitated infiltration of external fluids to the constantly moving and evolving reaction front at near static conditions.

Subsequent deformation of eclogite by dissolution-reprecipitation creep was accompanied by the development of a foliation and apparent grain coarsening. Both resulted in the observed reduction of grain boundary density and porosity, limiting fluid pathways to the fgpa. The reduced permeability likely inhibited the infiltration of retrograde fluid and subsequent dissolution-reprecipitation supported mineral replacement. Together with fast exhumation rates (Miller et al., 2005; Thöni et al., 2008), this likely resulted in the preservation of the metastable eclogitic mineral paragenesis during exhumation. The apparent contradiction between continuous high H$_2$O activity and simultaneous closure of fluid pathways can be explained by internal buffering of the

H_2O activity. When considering the assemblage garnet, omphacitic clinopyroxene, clinozoisite, kyanite, quartz and rutile equilibrated at peak conditions in presence of a fluid with $a(H_2O)$ close to one, removing the fluid from the system at constant P-T conditions produces H_2O at the expense of clinozoisite by reaction 1 (see Section 4.4) according to Le Chatelier's principle.

5.5. Rheological evolution during and after eclogitization

The analysis presented above indicates that mineralogical and volumetric changes caused by eclogitization of a metastable gabbro during peak metamorphic conditions resulted in accommodation of strain in eclogite of the Hohl locality. Strain localization at eclogite facies conditions in mafic protoliths has been extensively discussed (Jolivet et al., 2005; Terry and Heidelbach, 2006; Engvik et al., 2007; Austrheim, 2013; Zertani et al., 2019). While eclogitization analyzed in those studies is associated with brittle precursors or highly localized shear zones acting as channelized fluid pathways, we do not observe unambiguous correlation of fracturing, reaction front and strain localization. The mechanisms of strain weakening classically inferred from eclogite facies shear zones might therefore not be applicable in the case considered here. Our results allow us however to draw some implications regarding the mechanical evolution of the gabbro body of Hohl during and after eclogitization.

Mechanical weakening related to phase transformations has been suggested to be an important strain localization mechanism. Mechanical weakening is either promoted by the small grain size of newly formed minerals and activation of GBS (de Ronde et al., 2005; Hidas et al., 2013; Giuntoli et al., 2018; Stünitz et al., 2020) or by a transient increased dislocation activity (i.e. transformational plasticity; Sauveur, 1924; Winger et al., 1980; Schmidt et al., 2003).

We here propose an alternative model of mechanical evolution during eclogitization (Fig. 12), which is inspired by the generalized theoretical study on transformational plasticity by Poirier (1982). Our observations suggest that during eclogitization the first stages of deformation is accommodated by a combination of steady state creep and transient transformational creep. Both, steady state and transformational creep are driven by fluid influx and accommodated by dissolution-precipitation. Additionally, the unfavored energetic state of the metastable gabbro is likely to increase reaction rates and result in an increased transformational creep rate. The combination of both results in enhanced weakening, in comparison to the one related to steady-state creep alone. With ongoing mineral replacement, the volume fraction of eclogite increases and consequently the strain accommodated by steady state creep of the eclogite increases. Once all the protolith is transformed into eclogite, metamorphic reactions stop, the weakening effect induced by transformational creep cannot be active and eclogite then shows apparent hardening (Fig. 12). Nevertheless, eclogite deforming by steady-state creep is weaker than the initial gabbro protolith.

While the model presented here gives insights into the qualitative rheological evolution during eclogitization, it does not describe possible rheological changes during foliation development. In a high P and high T regime as the one experienced by the SKC, rocks are usually assumed to deform at high differential stresses by dislocation creep. In such a deformation regime, strong viscosity contrasts as anticipated for rocks in the SKC, result in strain partitioning where most of the strain is accommodated in the weaker matrix (e.g. Grigull et al., 2012). Even though the metasediments at SKC have accommodated a large part of the strain in the area of Hohl, the very development of the pronounced eclogitic foliation indicates that some tectonic strain was transferred from the surrounding weaker metasedimentary matrix to the stronger eclogite inclusion. Comparison with inclusion in matrix models (Schmid and Podladchikov, 2003) actually suggests that accommodation of tectonic strain in the eclogite was possible only if it had a viscosity less than 3 orders of magnitude larger than the one of the surrounding metasediment. This might have been a direct effect of active dissolution-
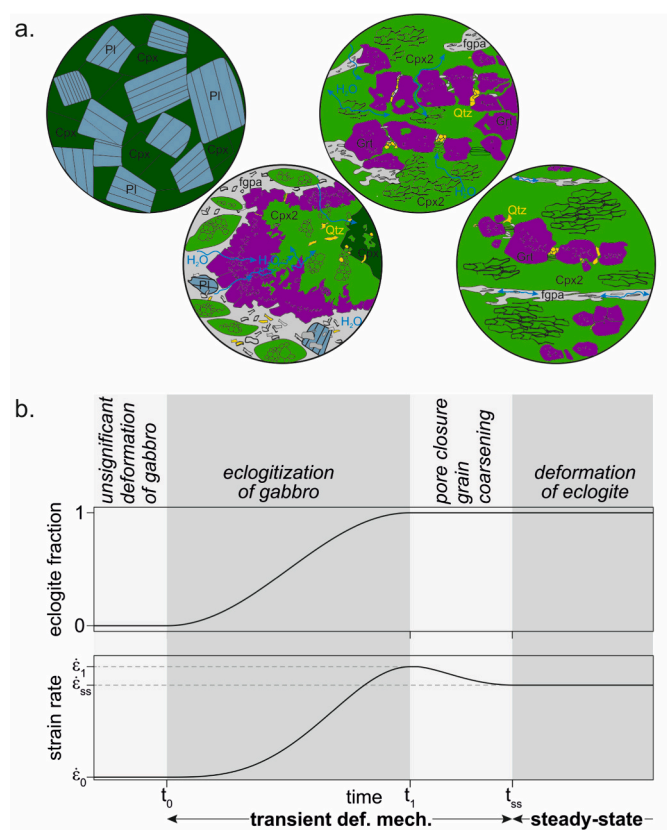

Fig. 12. Conceptual model showing the petrographic and microstructural evolution (a) and the corresponding strain rate evolution (b) at several stages of the metagabbro to eclogite transformation. t_0: onset of eclogitization, t_1: completed eclogitization, t_{ss}: onset of steady state deformation. All axes are unscaled. See Section 5.5. for explanation.

reprecipitation creep in eclogite that has lowered viscosity. In contrast to rocks deforming by dislocation creep where viscosity depends dominantly on the strength of the rock forming minerals (Huet et al., 2014 and references therein), the strength of rocks deforming by dissolution-reprecipitation creep additionally depends on grain size, distribution of interphase boundaries, chemical potential gradients and fluid supply (Wassmann and Stöckhert, 2013).

In the course of foliation development, we observe an apparent reduction of porosity, rearrangement of minerals and grain growth. As discussed in the previous section, all these processes induce a decrease of the amount of phase and grain boundaries and tend to close possible fluid pathways, consequently making dissolution-reprecipitation and diffusion creep less efficient and possibly causing some hardening (Fig. 12). Once deformation of omphacitic clinopyroxene and garnet by dissolution-reprecipitation and diffusion becomes less efficient most of the strain in eclogites is accommodated in layers of fine grained polyphase aggregate by phase boundary sliding and rigid body rotation (Cao et al., 2020; Zhao et al., 2019).

The presented data thus suggest a slightly controversial model for the interplay between deformation, fluid pathways and rheological behaviour. In accordance to previous studies our data suggest initial rheological weakening caused by fluids. However, here continuous deformation does not result in strain localization as often observed within the dislocation creep regime where enhanced grain size reduction via dynamic recrystallization processes is accompanied by continuous weakening (Platt and Behr, 2011; Rogowitz et al., 2014), localization of deformation and introduction of further fluid pathways (Fusseis et al., 2009; Gilgannon et al., 2017). Instead, deformation by dissolution-reprecipitation creep seems to result in grain coarsening followed by

subsequent strengthening. We hypothesize that deformation induced grain coarsening and reduction in fluid pathways might at later stage inhibit activation of dissolution-reprecipitation and diffusion creep. The subsequent strengthening effect results either in breaking of the rock (as observed in omphacitic clinopyroxene crystals at Hohl) or activation of dislocation creep. The latter is however quite speculative at this stage and needs further investigations.

5.6. Rheological implications for convergent settings

The deformation behaviour at plate interfaces plays an important role for large scale geodynamic processes. The geodynamic evolution of such convergent settings is highly governed by the rheology of the rocks occurring at the interface (Agard et al., 2018 and references therein). The transformation of a mafic protolith like gabbro, granulite and basalt into an eclogite at high to ultrahigh pressure suggests that the rheology of eclogite can be a parameter controlling at first order the formation and evolution of subduction and collision zones. Despite the necessity of a better understanding of the deformation behaviour of eclogite, its rheology is still highly debated. Extensive experimental studies suggest that both, omphacite and garnet are rather strong minerals in which dislocation creep is not active at differential stresses below 1 GPa (Li et al., 2006; Zhang et al., 2006; Mei et al., 2010; Moghadam et al., 2010). Similar observations have been made during experimental studies on synthetic eclogite (Jin et al., 2002; Zhang and Green, 2007).

To some extent the experimentally derived observation of a strong eclogitic mineral assemblage is at odds with the observation of localization of shear zones and mylonitization of eclogite (Engvik et al., 2007; Angiboust et al., 2011; Austrheim, 2013; Zertani et al., 2019). In contrast to deformation by dislocation creep, dissolution-reprecipitation creep is known to operate at low differential stress (Wassmann and Stöckhert, 2013, and references therein) in accordance to inferred stresses in subduction zones (Stöckhert and Renner, 1998). Microstructural characteristics of foliated eclogite from the outcrop of Hohl and especially the SPO and CPO of omphacitic clinpyroxene are similar to microstructures previously observed in mylonitic eclogite (Kurz et al., 2004; Kurz, 2005; Terry and Heidelbach, 2006; Engvik et al., 2007). Our investigations reveal that the eclogite from the outcrop of Hohl deformed dominantly by dissolution-reprecipitation creep, which is in contradiction with the common interpretation of the omphacite SPO and CPO that invokes dislocation creep and glide. A recent study (Stünitz et al., 2020) also describes microstructures usually linked to dislocation creep in eclogite deformed by low-stress diffusion creep.

This apparent contradiction emphasizes that special caution is needed when inferring active deformation mechanisms from eclogite microstructures. A correct interpretation of active deformation mechanisms and resulting rock rheology is crucial for defining the input parameter of large scale thermo-mechanical geodynamic models of convergence zones. So far, a power-law rheology corresponding to the dislocation creep regime is generally applied (Gerya, 2019 and references therein), which might overestimate the strength. In order to investigate the impact of our results on the evolution of convergent settings the calibration of creep parameter for the deformation of eclogite in the dissolution-precipitation creep regime is needed. We do not claim that dislocation creep does not occur in eclogite but recent studies suggest that, deformation by dissolution-reprecipitation or diffusion creep is more likely to occur, especially in subduction zones where large amounts of fluids are available (Piepenbreier and Stöckhert, 2001; Stünitz et al., 2020). Additionally, the rheological behaviour of the oceanic crust and lower continental crust in convergence setting might not be faithfully modeled by a constant set of parameters corresponding to basalt, gabbro or mafic granulite, if eclogitization occurs. Our observations suggest a transient rheological evolution with softening due to transformation strain during replacement of gabbro or mafic granulite by eclogite followed by apparent hardening once transformation is completed. Deformation induced reduction of fluid pathways and decreased efficiency of dissolution-reprecipitation creep is likely to cause further hardening of the eclogite whereas activation of dislocation creep would instead result in weakening.

6. Conclusion

Investigations on eclogitic Al-Mg-rich metagabbro along a deformation gradient sampled at the outcrop of Hohl (Saualpe-Koralpe Complex, Eastern Alps, Austria) yield the following results:

- Eclogitization occurred at peak conditions of 640 °C, 1.9–2.0 GPa in presence of a H_2O dominated fluid phase. The presence of fluid is a common feature related to the gabbro-eclogite transformation.
- The dominant mechanism allowing the formation and deformation of eclogite was dissolution-(re)precipitation.
- Distributed eclogitization was related to the development of a microporosity allowing fluids to migrate in an unchannelized way and controlled by dissolution of the metastable gabbro and precipitation of eclogitic minerals. This induced the development of a transient micro-porosity and efficient fluid pathways at eclogite facies conditions.
- The development of a foliation due to subsequent deformation at eclogite facies resulted in the development of a shape and crystallographic preferred orientation of omphacitic clinopyroxene in the dissolution-reprecipitation creep regime.
- The activation of dissolution-reprecipitation creep allowed continuous deformation of eclogite surrounded by metasediment.

These local results have implication on the processes active in mafic rocks at eclogite facies conditions:

- Fluid supported eclogitization of a metastable dry mafic rock at nearly static conditions results in the development of efficient fluid pathways at high pressure.
- Strain accommodation by dissolution-reprecipitation creep is accompanied by grain coarsening and can result in reduction of former fluid-pathways.
- Transformational and volumetric strain during fluid assisted eclogitization of a dry mafic protolith results in transient weakening and is followed by apparent hardening once eclogitization is completed.

Appendix A. Supplementary data

Supplementary data to this article can be found online at https://doi.org/10.1016/j.tecto.2021.229079.

References

Agard, P., Plunder, A., Angiboust, S., Bonnet, G., Ruh, J., 2018. The subduction plate interface: rock record and mechanical coupling (from long to short time scales). Lithos 320–321, 537–561.

Agard, P., Prigent, C., Soret, M., Dubacq, B., Guillot, S., Deldicque, D., 2020. Slabitization: Mechanisms controlling subduction development and viscous coupling. Earth Sci. Rev. 103259 https://doi.org/10.1016/j.earscirev.2020.103259.

Angiboust, S., Agard, P., Raimbourg, H., Yamato, P., Huet, B., 2011. Subduction interface processes recorded by eclogite-facies shear zones (Monviso, W. Alps). Lithos 127 (1–2), 222–238. https://doi.org/10.1016/j.lithos.2011.09.004.

Austrheim, H., 1987. Eclogitization of lower crustal granulites by fluid migration through shear zones. Earth Planet. Sci. Lett. 81 (2–3), 221–232. https://doi.org/10.1016/0012-821X(87)90158-0.

Austrheim, H., 2013. Fluid and deformation induced metamorphic processes around Moho beneath continent collision zones: examples from the exposed root zone of the Caledonian mountain belt, W-Norway. Tectonophysics 609 (0040), 620–635. https://doi.org/10.1016/j.tecto.2013.08.030.

Austrheim, H., Erambert, M., Engvik, A.K., 1997. Processing of crust in the root of the Caledonian continental collision zone: the role of eclogitization. Tectonophysics 273 (1–2), 129–153. https://doi.org/10.1016/S0040-1951(96)00291-0.

Austrheim, H., Dunkel, K.G., Plümper, O., Ildefonse, B., Liu, Y., Jamtveit, B., 2017. Fragmentation of wall rock garnets during deep crustal earthquakes. Sci. Adv. 3 (2) https://doi.org/10.1126/sciadv.1602067.

Bascou, J., Barruol, G., Vauchez, A., Mainprice, D., Egydio-Silva, M., 2001. EBSD-measured lattice-preferred orientations and seismic properties of eclogites. Tectonophysics 342 (1–2), 61–80. https://doi.org/10.1016/S0040-1951(01)00156-1.

Bascou, J., Tommasi, A., Mainprice, D., 2002. Plastic deformation and development of clinopyroxene lattice preferred orientations in eclogites. J. Struct. Geol. 24 (8), 1357–1368. https://doi.org/10.1016/S0191-8141(01)00137-7.

Brodie, K.H., Rutter, E.H., 1987. The role of transiently fine-grained reaction products in syntectonic metamorphism: natural and experimental examples. Can. J. Earth Sci. 24 (3), 556–564. https://doi.org/10.1139/e87-054.

Bruand, E., Stüwe, K., Proyer, A., 2010. Pseudosection modelling for a selected eclogite body from the Koralpe (Hohl), Eastern Alps. Mineral. Petrol. 99 (1), 75–87. https://doi.org/10.1007/s00710-009-0097-7.

Buatier, M., Van Roermund, H.L.M., Drury, M.R., Lardeaux, J.M., 1991. Deformation and recrystallization mechanisms in naturally deformed omphacites from the Sesia-Lanzo zone: geophysical consequences. Tectonophysics 195, 11–27.

Bunge, H.J., 1982. Texture Analysis in Materials Science: Mathematical Models. Butterworths, London.

Cao, Y., Du, J., Park, M., Jung, S., Park, Y., Kim, D., Austrheim, H., 2020. Metastability and nondislocation-based deformation mechanisms of the flem eclogite in the Western Gneiss Region, Norway. J. Geophys. Res. Solid Earth 125 (5), 1–33. https://doi.org/10.1029/2020JB019375.

de Capitani, C., Brown, T.H., 1987. The computation of chemical equilibrium in complex systems containing non-ideal solutions. Geochim. Cosmochim. Acta 51 (10), 2639–2652.

de Capitani, C., Petrakakis, K., 2010. The computation of equilibrium assemblage diagrams with Theriak/Domino software. Am. Mineral. 95 (7), 1006–1016.

de Ronde, A.A., Stünitz, H., Tullis, J., Heilbronner, R., 2005. Reaction-induced weakening of plagioclase–olivine composites. Tectonophysics 409 (1), 85–106.

Engvik, A.K., Austrheim, H., Erambert, M., 2001. Interaction between fluid flow, fracturing and mineral growth during eclogitization, and example from the Sunnfjord area, Western Gneiss Region, Norway. Lithos 57 (2–3), 111–141. https://doi.org/10.1016/S0024-4937(01)00037-8.

Engvik, Ane K., Andersen, T.B., Wachmann, M., 2007. Inhomogeneous deformation in deeply buried continental crust, an example from the eclogite-facies province of the Western Gneiss Region, Norway. Nor. Geol. Tidsskr. 87 (4), 373–389.

Evans, B., Renner, J., Hirth, G., 2001. A few remarks on the kinetics of static grain growth in rocks. Int. J. Earth Sci. 90 (1), 88–103.

Froitzheim, N., Pleuger, J., Roller, S., Nagel, T., 2003. Exhumation of high- and ultrahigh-pressure metamorphic rocks by slab extraction. Geology 31 (10), 925–928. https://doi.org/10.1130/G19748.1.

Fusseis, F., Regenauer-Lieb, K., Liu, J., Hough, R.M., De Carlo, F., 2009. Creep cavitation can establish a dynamic granular fluid pump in ductile shear zones. Nature 459 (7249), 974–977. https://doi.org/10.1038/nature08051.

Gardés, E., Wunder, B., Wirth, R., Heinrich, W., 2011. Growth of multilayered polycrystalline reaction rims in the MgO-SiO2 system, part I: experiments. Contrib. Mineral. Petrol. 161 (1), 1–12. https://doi.org/10.1007/s00410-010-0517-z.

Gardés, E., Wunder, B., Marquardt, K., Heinrich, W., 2012. The effect of water on intergranular mass transport: new insights from diffusion-controlled reaction rims in the MgO-SiO 2 system. Contrib. Mineral. Petrol. 164 (1), 1–16. https://doi.org/10.1007/s00410-012-0721-0.

Gerya, T., 2019. Introduction to Numericaal Geodynamic Modelling. Cambrige University Press.

Gifkins, R.C., 1976. Grain-boundary sliding and its accommodation during creep and superplasticity. Metall. Trans. A. 7 (7), 1225–1232.

Gilgannon, J., Fusseis, F., Menegon, L., Regenauer-Lieb, K., Buckman, J., 2017. Hierarchical creep cavity formation in an ultramylonite and implications for phase mixing. Solid Earth 8 (6), 1193–1209. https://doi.org/10.5194/se-8-1193-2017.

Giuntoli, F., Menegon, L., Warren, C.J., 2018. Replacement reactions and deformation by dissolution and precipitation processes in amphibolites. J. Metamorph. Geol. 36 (9), 1263–1286.

Goncalves, P., Poilvet, J.C., Oliot, E., Marquer, D., 2016. How does shear zone nucleate ? An example from the Suretta nappe. J. Struct. Geol. 86, 166–180.

Green, E.C.R., White, R.W., Diener, J.F.A., Powell, R., Holland, T.J.B., Palin, R.M., 2016. Activity–composition relations for the calculation of partial melting equilibria in metabasic rocks. J. Metamorph. Geol. 34 (9), 845–869.

Gregurek, D., Abart, R., Hoinkes, G., 1997. Contrasting eoalpine PT evolutions in the southern Koralpe, Eastern Alps. Mineral. Petrol. 60 (1), 61–80.

Griggs, D., 1967. Hydrolytic Weakening of Quartz and Other Silicates*, 506, pp. 19–31.

Griggs, D.T., Paterson, M.S., Heard, H.C., Turner, F.J., 1960. Annealing recrystallization in calcite crystals and aggregates. In: Rock De- formation. Geol. Soc. Am. Mem. 79, 21–37.

Grigull, S., Krohe, A., Moos, C., Wassmann, S., Stöckhert, B., 2012. "Order from chaos": a field-based estimate on bulk rheology of tectonic mélanges formed in subduction zones. Tectonophysics 568, 86–101.

Habler, G., Thöni, M., 2001. Preservation of Permo–Triassic low-pressure assemblages in the Cretaceous high-pressure metamorphic Saualpe crystalline basement (Eastern Alps, Austria). J. Metamorph. Geol. 19, 679–697.

Haüy, R.-J., 1822. Traité de miné ralogie. In: revue, corrigée et considé rablement augmentée par l'auteur, Seconde édition. Bachelier et Huzard, Paris. 4 Vols+atlas (t. II, p. 456; t. IV, p. 548).

Helmstaedt, H., Anderson, O., Gavasci, A., 1972. Petrofabric studies of eclogite, spinel-websterite and spinel-lherzolite xenoliths from kimberlite bearing breccia pipes in southeastern Utah and northeastern Arizona. J. Geophys. Res. 47, 4350–4365.

Hidas, K., Garrido, C.J., Tommasi, A., Padrón-Navarta, J.A., Thielmann, M., Konc, Z., Marchesi, C., 2013. Strain localization in pyroxenite by reaction-enhanced softening in the shallow subcontinental lithospheric mantle. J. Petrol. 54 (10), 1997–2031.

Holland, T., Powell, R., 2003. Activity–composition relations for phases in petrological calculations: an asymmetric multicomponent formulation. Contrib. Mineral. Petrol. 145 (4), 492–501.

Holland, T.J.B., Powell, R., 2011. An improved and extended internally consistent thermodynamic dataset for phases of petrological interest, involving a new equation of state for solids. J. Metamorph. Geol. 29 (3), 333–383.

Huet, B., Yamato, P., Grasemann, B., 2014. The Minimized Power Geometric model : an analytical mixing model for calculating polyphase rock viscosities consistent. J. Geophys. Res. Solid Earth. https://doi.org/10.1002/2013JB010453.Abstract.

Jamtveit, B., Bucher-Nurminen, K., Austrheim, H., 1990. Fluid controlled eclogitization of granulites in deep crustal shear zones, Bergen arcs, Western Norway. Contrib. Mineral. Petrol. 104 (2), 184–193. https://doi.org/10.1007/BF00306442.

Jamtveit, B., Petley-Ragan, A., Incel, S., Dunkel, K.G., Aupart, C., Austrheim, H., Renard, F., 2019. The effects of earthquakes and fluids on the metamorphism of the Lower Continental crust. J. Geophys. Res. Solid Earth 124 (8), 7725–7755. https://doi.org/10.1029/2018JB016461.

Jin, Z.M., Zhang, J., Green, I.W., Jin, S., 2002. Eclogite rheology: Implication for subducted lithosphere. Geology 29 (8), 667–670. https://doi.org/10.1130/0091-7613(2001)029<0667:ERIFSL>2.0.CO.

John, T., Schenk, V., 2003. Partial eclogitisation of gabbroic rocks in a late Precambrian subduction zone (Zambia): Prograde metamorphism triggered by fluid infiltration. Contrib. Mineral. Petrol. 146 (2), 174–191. https://doi.org/10.1007/s00410-003-0492-8.

Jolivet, L., Raimbourg, H., Labrousse, L., Avigad, D., Leroy, Y., Austrheim, H., Andersen, T.B., 2005. Softening trigerred by eclogitization, the first step toward exhumation during continental subduction. Earth Planet. Sci. Lett. 237 (3–4), 532–547. https://doi.org/10.1016/j.epsl.2005.06.047.

Keller, L.M., Abart, R., Wirth, R., Schmid, D.W., Kunze, K., 2006. Enhanced mass transfer through short-circuit diffusion: growth of garnet reaction rims at eclogite facies conditions. Am. Mineral. 91 (7), 1024–1038. https://doi.org/10.2138/am.2006.2068.

Keller, L.M., Wirth, R., Rhede, D., Kunze, K., Abart, R., 2008. Asymmetrically zoned reaction rims: assessment of grain boundary diffusivities and growth rates related to natural diffusion-controlled mineral reactions. J. Metamorph. Geol. 26 (1), 99–120. https://doi.org/10.1111/j.1525-1314.2007.00747.x.

Keppler, R., 2018. Crystallographic preferred orientations in eclogites – A review. Journal of Structural Geology 115, 284–296. https://doi.org/10.1016/j.jsg.2018.04.003.

Kurz, W., 2005. Constriction during exhumation: evidence from eclogite microstructures. Geology 33 (1), 37–40. https://doi.org/10.1130/G20887.1.

Kurz, W., Fritz, H., Tenczer, V., Unzog, W., 2002. Tectonometamorphic evolution of the Koralm Complex (Eastern Alps): constraints from microstructures and textures of the Plattengneis shear zone. J. Struct. Geol. 24, 1957–1970.

Kurz, W., Jansen, E., Hundenborn, R., Pleuger, J., Schäfer, W., Unzog, W., 2004. Microstructures and crystallographic preferred orientations of omphacite in Alpine eclogites: implications for the exhumation of (ultra-) high-pressure units. J. Geodyn. 37 (1), 1–55. https://doi.org/10.1016/j.jog.2003.10.001.

Labrousse, L., Hetényi, G., Raimbourg, H., Jolivet, L., Andersen, T.B., 2010. Initiation of crustal-scale thrusts triggered by metamorphic reactions at depth: insights from a comparison between the Himalayas and Scandinavian Caledonides. Tectonics 29 (5). https://doi.org/10.1029/2009TC002602.

Li, L., Long, H., Raterron, P., Weidner, D., 2006. Plastic flow of pyrope at mantle pressure and temperature. Am. Mineral. 91 (4), 517–525. https://doi.org/10.2138/am.2006.1913.

Mancktelow, N.S., Pennacchioni, G., 2005. The control of precursor brittle fracture and fluid–rock interaction on the development of single and paired ductile shear zones. J. Struct. Geol. 27 (4), 645–661. https://doi.org/10.1016/j.jsg.2004.12.001.

Mancktelow, N.S., Grujic, D., Johnson, E.L., 1998. An SEM study of porosity and grain boundary microstructure in quartz mylonites, Simplon Fault Zone, Central Alps. Contrib. Mineral. Petrol. 131 (1), 71–85. https://doi.org/10.1007/s004100050379.

Mauler, Alexandra, Godard, Gaston, Kunze, Karsten, 2001. Crystallographic fabrics of omphacite, rutile and quartz in Vendée eclogites (Armorican Massif, France): Consequences for deformation mechanisms and regimes. Tectonophysics 342 (1-2), 81–112.

Martin, J.W., Doherty, R.D., Cantor, 1997. Stability of Microstructure in Metallic Systems. Cambridge University Press, Cambridge.

Mei, S., Suzuki, A.M., Kohlstedt, D.L., Xu, L., 2010. Experimental investigation of the creep behavior of garnet at high temperatures and pressures. J. Earth Sci. 21 (5), 532–540. https://doi.org/10.1007/s12583-010-0127-8.

Menegon, Luca, Pennacchioni, G., Spiess, R., 2008. Dissolution-precipitation creep of K-feldspar in mid-crustal granite mylonites. J. Struct. Geol. 30 (5), 565–579. https://doi.org/10.1016/j.jsg.2008.02.001.

Menegon, L., Pennacchioni, G., Malaspina, N., Harris, K., Wood, E., 2017. Earthquakes as precursors of ductile shear zones in the dry and strong Lower Crust. Geochem. Geophys. Geosyst. 18 (12), 4356–4374. https://doi.org/10.1002/2017GC007189.

Milke, R., Dohmen, R., Becker, H.W., Wirth, R., 2007. Growth kinetics of enstatite reaction rims studied on nano-scale, part I: methodology, microscopic observations and the role of water. Contrib. Mineral. Petrol. 154 (5), 519–533. https://doi.org/10.1007/s00410-007-0207-7.

Miller, C., 1990. Petrology of the type locality eclogites from the Koralpe and Saualpe (Eastern Alps), Austria. Schweiz. Mineral. Petrogr. Mitt. 70 (2), 287–300.

Miller, C., Thöni, M., 1997. Eo-Alpine eclogitisation of Permian MORB-type gabbros in the Koralpe (Eastern Alps, Austria): new geochronological, geochemical and petrological data. Chem. Geol. 137 (3–4), 283–310. https://doi.org/10.1016/S0009-2541(96)00165-9.

Miller, C., Stosch, H.G., Hoernes, S., 1988. Geochemistry and origin of eclogites from the type locality Koralpe and Saualpe, Eastern Alps, Austria. Chem. Geol. 67 (1–2), 103–118.

Miller, C., Thöni, M., Konzett, J., Kurz, W., Schuster, R., 2005. Geology of the Saualpe-Koralpe region. Mitteil. Österreich. Mineral. Gesellsc. 150, 227–263.

Miller, C., Zanetti, A., Thöni, M., Konzett, J., 2007. Trace element mineral chemistry of the type locality (Koralpe, Saualpe) and Pohorje eclogites (Eastern Alps): implications for behaviour of fluid-mobile elements in a continental subduction zone, geochronology and geothermometry. Chem. Geol. 239, 96–123.

Moghadam, R.H., Trepmann, C.a., Stöckhert, B., Renner, J., 2010. Rheology of synthetic omphacite aggregates at high pressure and high temperature. J. Petrol. 51 (4), 921–945. https://doi.org/10.1093/petrology/egq006.

Mørk, M.B.E., 1985. A gabbro to eclogite transition on Flemsøy, Sunnmøre, West Norway. Chem. Geol. 50, 283–310.

Mullin, J.W., 2001. Crystallization. Elsevier.

Ostwald, W., 1900. Über die vermeintliche Isomerie des roten und gelben Quecksilberoxyds und die Oberflächenspannung fester Körper. Zeit. Phys. Chem. Stöch. metr. Verwandsc. 34, 495–503.

Palin, Richard M., et al., 2016. High-grade metamorphism and partial melting of basic and intermediate rocks. Journal of Metamorphic Geology 34 (9), 871–892.

Pennacchioni, G., 1996. Progressive eclogitization under fluid-present conditions of pe-Alpine mafic granulites in the Austroalpine Mt Emilius Klippe (Italian Western Alps). J. Struct. Geol. 18 (5), 549–561.

Petley-Ragan, A., Dunkel, K.G., Austrheim, H., Ildefonse, B., Jamtveit, B., 2018. Microstructural records of earthquakes in the lower crust and associated fluid-driven metamorphism in plagioclase-rich granulites. J. Geophys. Res. Solid Earth 123 (5), 3729–3746. https://doi.org/10.1029/2017JB015348.

Petrakakis, K., Dietrich, H., 1985. MINSORT: a program for the processing and archivation of microprobe analyses of silicate and oxide minerals. Neues J. Minera. Monat. 8, 379–384.

Piepenbreier, D., Stöckhert, B., 2001. Plastic flow of omphacite in eclogites at temperatures below 500 C–implications for interplate coupling in subduction zones. Int. J. Earth Sci. 90 (1), 197–210.

Platt, J.P., Behr, W.M., 2011. Grainsize evolution in ductile shear zones: implications for strain localization and the strength of the lithosphere. J. Struct. Geol. 33 (4), 537–550.

Plunder, A., Agard, P., Dubacq, B., Chopin, C., Bellanger, M., 2012. How continuous and precise is the record of P–T paths? Insights from combined thermobarometry and thermodynamic modelling into subduction dynamics (Schistes Lustrés, W. Alps). J. Metamorph. Geol. 30 (3), 323–346.

Poirier, J.P., 1982. On transformation plasticity. J. Geophys. Res. Solid Earth 87 (B8), 6791–6797.

Proyer, A., Postl, W., 2010. Eclogitized Gabbros from Gressenberg, Koralpe, Austria: transformation phenomena and their interpretation. Mitteil. Nat. Vereines Steiermark 140, 45–67.

Putnis, A., Austrheim, H., 2010. Fluid-induced processes: Metasomatism and metamorphism. Geofluids 10 (1–2), 254–269. https://doi.org/10.1111/j.1468-8123.2010.00285.x.

Putnis, A., Putnis, C.V., 2007. The mechanism of reequilibration of solids in the presence of a fluid phase. J. Solid State Chem. 180 (5), 1783–1786. https://doi.org/10.1016/j.jssc.2007.03.023.

Putnis, A., Jamtveit, B., Austrheim, H., 2017. Metamorphic processes and seismicity: the Bergen Arcs as a natural laboratory. J. Petrol. 58 (10), 1871–1898. https://doi.org/10.1093/petrology/egx076.

Putz, M., Stüwe, K., Jessell, M., Calcagno, P., 2006. Three-dimensional model and late stage warping of the Plattengneis Shear Zone in the Eastern Alps. Tectonophysics 412 (1–2), 87–103.

Raimbourg, H., Jolivet, L., Labrousse, L., Leroy, Y., Avigad, D., 2005. Kinematics of syneclogite deformation in the Bergen Arcs, Norway: implications for exhumation mechanisms. Geol. Soc. Lond., Spec. Publ. 243 (1), 175–192. https://doi.org/10.1144/GSL.SP.2005.243.01.13.

Rogowitz, A., Grasemann, B., Huet, B., Habler, G., 2014. Strain rate dependent calcite microfabric evolution – an experiment carried out by nature. J. Struct. Geol. 69, 1–17.

Sauveur, A., 1924. What is steel? Another answer. Iron Age 113, 581.

Schuster, Ralf, Stüwe, Kurt, 2008. Permian metamorphic event in the Alps. Geology 36 (8), 603–606.

Schmid, D.W., Podladchikov, Y.Y., 2003. Analytical solutions for deformable elliptical inclusions in general shear. Geophys. J. Int. 155 (1), 269–288.

Schmidt, C., Bruhn, D., Wirth, R., 2003. Experimental evidence of transformation plasticity in silicates: minimum of creep strength in quartz. Earth Planet. Sci. Lett. 205 (3–4), 273–280.

Schorn, S., 2018. Dehydration of metapelites during high-P metamorphism: the coupling between fluid sources and fluid sinks. J. Metamorph. Geol. 36 (3), 369–391.

Schorn, S., Diener, J.F.a., 2017. Details of the gabbro-to-eclogite transition determined from microtextures and calculated chemical potential relationships. J. Metamor. Geol. 55–75. https://doi.org/10.1111/jmg.12220.

Schorn, S., Stüwe, K., 2016. The Plankogel detachment of the Eastern Alps: petrological evidence for an orogen-scale extraction fault. J. Metamorph. Geol. 34 (2), 147–166. https://doi.org/10.1111/jmg.12176.

Schott, J., Brantley, S., Crerar, D., Guy, C., Borcsik, M., Willaime, C., 1989. Dissolution kinetics of strained calcite. Geochem. Cosmochim. Acta. 53, 373–382.

Schulz, B., 2017. Polymetamorphism in garnet micaschists of the Saualpe Eclogite Unit (Eastern Alps, Austria), resolved by automated SEM methods and EMP–Th–U–Pb monazite dating. J. Metamorph. Geol. 35 (2), 141–163. https://doi.org/10.1111/jmg.12224.

Segall, P., Simpson, C., 1986. Nucleation of ductile shear zones on dilatant fractures. Geology 14 (1), 56–59. https://doi.org/10.1130/0091-7613(1986)14<56:NODSZO>2.0.CO.

Stöckhert, B., Renner, J., 1998. Rheology of crustal rocks at ultrahigh pressure. In: When Continents Collide: Geodynamics and Geochemistry of Ultrahigh-Pressure Rocks. Springer, Dordrecht, pp. 57–95.

Stünitz, H., Tullis, J., 2001. Weakening and strain localization produced by syn-deformational reaction of plagioclase. Int. J. Earth Sci. 90 (1), 136–148. https://doi.org/10.1007/s005310000148.

Stünitz, H., Neufeld, K., Heilbronner, R., Finstad, A.K., Konopásek, J., Mackenzie, J.R., 2020. Transformation weakening: diffusion creep in eclogites as a result of interaction of mineral reactions and deformation. J. Struct. Geol. 139 (July) https://doi.org/10.1016/j.jsg.2020.104129.

Stüwe, K., Schuster, R., 2010. Initiation of subduction in the Alps: continent or ocean? Geology 38, 175–178.

Tasaka, M., Zimmerman, M.E., Kohlstedt, D.L., 2017. Rheological weakening of olivine+orthopyroxene aggregates due to phase mixing: 1. Mechanical behavior. Journal of Geophysical Research: Solid Earth 122 (10), 7584–7596.

Tenczer, V., Stüwe, K., 2003. The metamorphic field gradient in the eclogite type locality, Koralpe region, Eastern Alps. J. Metamorph. Geol. 21 (4), 377–393.

Terry, M.P., Heidelbach, F., 2006. Deformation-enhanced metamorphic reactions and the rheology of high-pressure shear zones, Western Gneiss Region, Norway. J. Metamorph. Geol. 24 (1), 3–18. https://doi.org/10.1111/j.1525-1314.2005.00618.x.

Thöni, M., 2006. Dating eclogite-facies metamorphism in the Eastern Alps–approaches, results, interpretations: a review. Mineral. Petrol. 88 (1–2), 123–148.

Thöni, M., Jagoutz, E., 1992. Some new aspects of dating eclogites in orogenic belts: Sm-Nd, Rb-Sr, and Pb-Pb iso- topic results from the Austroalpine Saualpe and Koralpe type-locality (Carinthia/Styria, southeastern Austria). Geochim. Cosmochim. Acta 56, 347–368.

Thöni, M., Miller, C., Blichert-Toft, J., Whitehouse, M., Konzett, J., Zanetti, A., 2008. Timing of high-pressure metamorphism and exhumation of the eclogite type-locality (Kupplerbrunn–Prickler Halt, Saualpe, south-eastern Austria): constraints from correlations of the Sm–Nd, Lu– Hf, U–Pb and Rb–Sr isotopic systems. J. Metam. Geol. 26, 561–581.

Tropper, P., Kunze, R., Manning, C.E., 2008. Experimental constraints on the role of brines in thetransformation of gabbros to eclogites: a case study fromthe Bärofen metagabbros (Koralpe, Styria). J. Alpine Geol. Gesellsc. Geol. Bergbaustud. Öster. 49, 113.

Warren, J.M., Hirth, G., 2006. Grain size sensitive deformation mechanisms in naturally deformed peridotites. Earth Planet. Sci. Lett. 248 (1–2), 438–450. https://doi.org/10.1016/j.epsl.2006.06.006.

Wassmann, S., Stöckhert, B., 2013. Rheology of the plate interface - Dissolution precipitation creep in high pressure metamorphic rocks. Tectonophysics 608, 1–29. https://doi.org/10.1016/j.tecto.2013.09.030.

White, R.W., Powell, R., Holland, T.J.B., Johnson, T.E., Green, E.C.R., 2014. New mineral activity–composition relations for thermodynamic calculations in metapelitic systems. J. Metamorph. Geol. 32 (3), 261–286.

Whitney, D.L., Evans, B.W., 2010. Abbreviations for names of rock-forming minerals. Am. Mineral. 95 (1), 185–187.

Wiesinger, M., Neubauer, F., Handler, R., 2006. Exhumation of the Saualpe eclogite unit, Eastern Alps: constraints from 40 Ar/39 Ar ages and structural investigations. Mineral. Petrol. 88 (1–2), 149–180.

Winger, L.A., Bradt, R.C., Hoke, J.H., 1980. Transformational Superplasticity of Bi2WO6 and Bi2M0O6. J. Am. Ceram. Soc. 63, 291–294.

Wintsch, R.P., 1980. The possible effects of deformation on chemical processes in metamorphic fault zones. In: AdvancesinPhysical Geochemistry, 4. Springer-Verlag, New York, USA.

Zertani, S., Labrousse, L., John, T., Andersen, T.B., Tilmann, F., 2019. The interplay of eclogitization and deformation during deep burial of the lower continental crust—a case study from the Bergen Arcs (Western Norway). Tectonics 38 (3), 898–915. https://doi.org/10.1029/2018TC005297.

Zhang, J., Green, H.W., 2007. Experimental investigation of eclogite rheology and its fabrics at high temperature and pressure. J. Metamorph. Geol. 25 (2), 97–115. https://doi.org/10.1111/j.1525-1314.2006.00684.x.

Zhang, J., Green, H.W., Bozhilov, K.N., 2006. Rheology of omphacite at high temperature and pressure and significance of its lattice preferred orientations. Earth Planet. Sci. Lett. 246 (3–4), 432–443. https://doi.org/10.1016/j.epsl.2006.04.006.

Zhao, N., Hirth, G., Cooper, R.F., Kruckenberg, S.C., Cukjati, J., 2019. Low viscosity of mantle rocks linked to phase boundary sliding. Earth Planet. Sci. Lett. 517, 83–94. https://doi.org/10.1016/j.epsl.2019.04.019.